GLASSY STATE BEHAVIOR IN CERAMIC SUPERCONDUCTORS

by

Atılgan Altınkök

THESIS SUBMITTED TO
THE GRADUATE SCHOOL OF NATURAL AND APPLIED SCIENCES
OF
THE ABANT İZZET BAYSAL UNIVERSITY
IN PARTIAL FULFILLMENT OF THE REQUIREMENTS FOR THE DEGREE
OF
MASTER OF SCIENCE
IN
THE DEPARTMENT OF PHYSICS

July 2004

Approval of the Graduate School of Natural and Applied Sciences

Prof. Dr. Davut KÖŞKER

Director

I certify that this thesis satisfies all the requirements as a thesis for the degree of Master of Science.

Prof. Dr. Ahmet Turan ALAN

Head of Physics Department

This is to certify that we have read this thesis and that in our opinion it is fully adequate, in scope and quality, as a thesis for the degree of Master of science.

Assoc. Prof. Dr. Kıvılcım KILIÇ

Supervisor

Examining Commitee Members

1. Prof. Dr. Mehmet CANKURTARAN

2. Assoc. Prof. Dr. Kıvılcım KILIÇ

3. Prof. Dr. Atilla KILIÇ

ABSTRACT

GLASSY STATE BEHAVIOR IN CERAMIC SUPERCONDUCTORS

Altınkök, Atılgan
Master of Science, Department of Physics
Supervisor: Assoc. Prof. Dr. Kıvılcım KILIÇ

July 2004, 86 pages

Strong non-linear dynamic responses developing due to the magnitude and type of driving current in bulk polycrystalline superconducting $Y_1Ba_2Cu_2O_{7-\delta}$ samples were investigated via the time evolution of the sample voltage, the V - t curves. The evolution of nonlinear V - t curves, including several novel types of dynamic changes induced by the transport current, were interpreted mainly by the spatial re-organization of the transport current in a multiply connected network of weak-link structure and glassy state relaxation. In addition, the influence of both the bidirectional square wave current and dc current on the evolution of the V - t curves was studied. In well-defined ranges of amplitudes and periods of driving current and temperatures, it was found that the non-linear response in V - t curves to low frequency driving current reflects itself as pronounced regular sinusoidal-type voltage oscillations. The current-induced regular sinusoidal-type voltage oscillations were interpreted in terms of the defective flow of current-induced self-magnetic flux (SMF) lines in a multiply connected network, semi-elastic coupling between SMF lines, and pinning centers. The oscillating mode was also discussed on the basis of the similarity between the flux dynamics and the charge density waves. The experimental techniques introduced in this study provides a useful tool to observe the time variation of the superconducting order parameter.

Keywords: Type–II superconductors, high-T_c ceramic superconductors, $Y_1Ba_2Cu_2O_{7-\delta}$, magnetization, critical current, relaxation, flux dynamics, superconducting order parameter.

ÖZET

SERAMİK SÜPERİLETKENLERDE CAMSI DURUM DAVRANIŞI

Altınkök, Atılgan

Yüksek Lisans, Fizik Bölümü

Tez Danışmanı: Doç. Dr. Kıvılcım Kılıç

Temmuz 2004, 86 sayfa

Süperiletken $Y_1Ba_2Cu_3O_{7-\delta}$ hacimli polikristal örneğinden sürülen akımın türüne ve büyüklüğüne bağlı olarak gelişen doğrusal olmayan kuvvetli dinamik tepkiler, örnek voltajının zaman değişimi ($V-t$ eğrileri) yoluyla incelendi. Taşıma akımı tarafından indüklenen dinamik değişimlerin çeşitli yeni tiplerini içeren doğrusal olmayan $V-t$ eğrilerinin gelişimi, esas olarak, zayıf eklem yapısının çoklu ağı içerisinde, taşıma akımının yerel olarak yeniden organizasyonu ve camsı durum durulması ile açıklandı. Ayrıca, iki yönlü kare dalga akımının ve dc akımının $V-t$ eğrilerinin gelişimine etkileri incelendi. Örnekten sürülen akımın genliği ve periyodu ile sıcaklığın iyi tanımlanmış değerlerinde, düşük frekanslı sürücü akıma karşı $V-t$ eğrilerindeki doğrusal olmayan tepkinin bazen kendini düzenli, sinuzoidal türde voltaj osilasyonları olarak yansıttığı bulundu. Akım tarafından indüklenmiş düzenli sinuzoidal türdeki voltaj osilasyonları, çoklu bağlantılı bir ağda, akımdan kaynaklanan öz-manyetik alan çizgilerinin kusurlu akışına ve öz-

manyetik akı çizgileri ile akı tutma merkezleri arasındaki yarı-esnek çiftlenime dayanılarak yorumlandı. Salınım modu, ayrıca, akı dinamiği ve yük yoğunluğu dalgaları arasındaki benzerliğe dayanılarak da tartışıldı. Bu çalışmada sunulan deneysel teknikler, süperiletkenlik düzen parametresinin zamanla değişimini gözlemek için kullanılışlı bir yöntem oluşturmaktadır.

Anahtar Kelimeler: Tip-II süperiletkenler, yüksek - T_c seramik süperiletkenler, $Y_1Ba_2Cu_2O_{7-\delta}$, mıknatıslanma, kritik akım, durulma, akı dinamiği, süperiletkenlik düzen parametresi.

ACKNOWLEDGEMENTS

I would first like to thank my supervisor, Assoc. Prof. Dr. Kıvılcım Kılıç, for her advice and support. She has been an ideal supervisor providing insightful comments and constructive criticism throughout this MSc. thesis. I feel very fortunate to have been her student.

I would also like to thank Prof. Dr. Atilla Kılıç, who introduced me to superconductivity and measurements at low temperatures. I have benefited greatly from many useful discussions we have had.

I am grateful to Hakan Yetiş and Assoc. Prof. Dr. Oktay Çetin, working with them has been stimulating and helpfull.

I would like to thank my colleagues and teachers, who was always friendly and supportive.

I would like to thank to my wife, who have unconditionally stayed encouraging me even the worst moment.

I owe great deal of gratitude to my parents, for supporting totally and unconditionally throughout my university years. My beliefs and values have been shaped in large part their influence.

This work is dedicated to memory of my grandfather Hüseyin Kama who passed away March 3, 2000. He was always a source of security and advice and will be missed forever.

TABLE OF CONTENTS

LIST OF FIGURES

CHAPTER 1

INTRODUCTION

Superconductivity was first discovered in 1911 by Kamerlingh Onnes. He noticed that the resistivity of Hg metal vanished abruptly at about 4.2 K. After the discovery of superconductivity, a search for superconducting materials with higher transition temperatures T_c has began. In 1986, a new class of the superconductors, High Temperature Superconductors (HTSC), was synthesized starting with the discovery of the superconductivity at ~ 35 K by Bednorz and Müller [1]. Soon after the discovery by Bednorz and Müller, a new class of HTSC called $YBa_2Cu_3O_{7-\delta}$ was found to have a critical temperature (T_c) of 92 K [10]. The high transition temperatures of the new superconductors opened expectations associated with their technical application, since these superconducting compounds only require easily accessible liquid nitrogen cooling at 77 K, rather than the more expensive liquid helium cooling. In Bednorz and Müller's remarkable pioneering paper [1], they introduced not only a new class of superconductors but also some of the key concepts with which the electrical and magnetic properties of these materials could be understood.

It is now well established that the magnetic and transport properties of HTSC are rather different from those of the conventional Type-II superconductors [3]. HTSC have layered structures with some two dimensional behavior, their coherence lengths are approaching interatomic distances, their pairing mechanism seems to be d-wave rather than s-wave. Their physical properties are highly anisotropic and fluctuation effects are fairly prominent due to their relatively high critical temperatures. Their pinning properties are also different from that of the conventional superconductors. In addition to the classical pinning mechanism, theoretical and experimental studies reveal the presence of an intrinsic pinning mechanism due to the layered structure [4]. These properties reflect themselves in both transport and magnetic measurements as fast relaxation in magnetization, broadening in resistance in the presence of an external magnetic field, low current carrying capacity due to the low pinning energy, current/field sweep rate dependence of current-voltage and magnetization curves, etc. [5].

The description of the flux motion in high temperature superconductors is a complicated and interesting problem. Therefore, many efforts have been carried out in order to understand their unusual properties such as history dependent time effects, strong metastability, slow voltage oscillations including memory effects, [5-8]. The aim of this study was to investigate the glassy state properties of polycrystalline bulk superconducting $Y_1Ba_2Cu_2O_{7-\delta}$ (YBCO) material at different temperatures which is associated with the quenched state created by interrupting the driving current or reducing it to a finite value. Another aim of this study was to assess the influence of dc current and bidirectional square wave current with long period on the time evolution of the sample voltage at various temperatures.

The rest of the thesis is organized as follows: In chapter two, it is intended to give a brief overview of the basic concepts of superconductivity. In chapter three, the glassy state relaxation is introduced. In chapter four, the details of sample preparation and experimental set-up are given. In chapter five, the experimental results on the glassy state, and the central role of dc and bi-directional driving currents are presented. In chapter six, the experimental results are discussed and compared to the theoretical models outlined in chapter three. Finally, in chapter seven, the results and findings of this work are summarized.

CHAPTER 2

SUPERCONDUCTIVITY

2.1 Brief History of Superconductivity

H.Kamerlingh Onnes, after his first liquefaction of helium, investigated the electrical resistance of metals at low temperatures. He observed that as mercury was cooled below a critical temperature, its resistivity vanished abruptly (Figure 2.1). This interesting state was called a *superconducting state* by Onnes. Subsequently many metals, alloys and intermetallic compounds have been shown to become superconducting, except alkali metals, alkaline-earth and magnetically ordered metals.

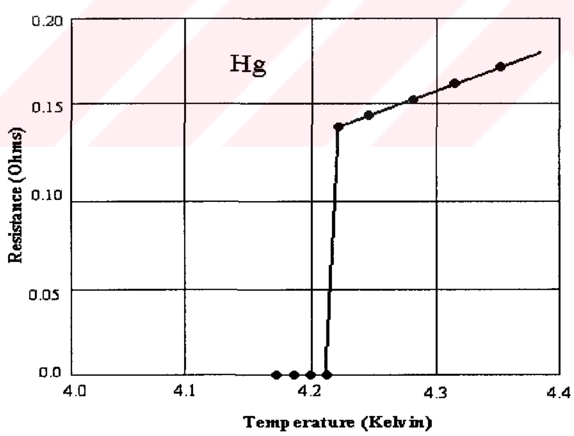

Figure 2.1 Superconducting transition of mercury [9].

The metal with the highest transition temperature (T_c = 9.2 K) is Niobium (Nb). The search for materials with higher transition temperatures led to the investigation of other alloys and compounds. A new class intermetallic compound Nb_3Sn with a critical temperature (T_c) of 18 K was found. Among the intermetallic compounds, Nb_3Ge with T_c ~23.2 K was discovered in 1973, which held the record of the highest T_c before the discovery of high temperature superconducting oxides [10].

In 1986, Bednorz and Müller found that the ceramic samples of $La_{2-x}Ba_xCuO_4$ (LBCO) had a T_c of about 35 K for x ≈ 0.15 [1]. LBCO is the first high temperature superconductor (HTSC) that has a layered perovskite structure. Further efforts have been carried out by many research groups to raise the critical temperature even more than that of LBCO. After several structural refinements, in 1987, $YBa_2Cu_3O_{7-\delta}$ ($\delta \approx 0.1$) was found to have a T_c of 92 K [2]. This significant discovery encouraged the scientist to search other possible HTSCs. Within a very short time, the Bi-Sr-Ca-Cu-O system with its two superconducting main phases was discovered: One of them is classified as $Bi_2Sr_2Ca_1Cu_2O_{8+y}$ (Bi-2212) phase with T_c = 85 K, and, the other is $Bi_2Sr_2Ca_2Cu_3O_{10+y}$ (Bi-2223) phase with T_c =110 K [11]. Then, $Tl_2Ba_2Ca_2Cu_3O_{10}$ was discovered with T_c approximately 125 K [12]. After the synthesization of Tl-based ceramic superconductors, another superconducting ceramic, $HgBa_2Ca_2Cu_3O_{8+y}$ with T_c of 133 K was found [14]. In the mean time, it was discovered that the C_{60} molecule becomes superconducting when it is doped with alkali atoms such as K, Rb and Cs. The highest reported T_c among the fullerens is 40 K for Cs_3C_{60} [15].

Magnesium Diboride (MgB_2) was discovered to become superconducting below about 40 K in January 2001 [16]. MgB_2 is an inter-metallic compound with remarkable high transition temperature as compared to that of conventional ones. Detailed studies on MgB_2 revealed that it has many advantages due to the lower anisotropy, larger coherence length, and transparency of grain boundaries to electrical current flow and, therefore, it is a very promising material for practical applications [17].

2.2 Structural Properties of $YBa_2Cu_3O_{7-\delta}$

$YBa_2Cu_3O_{7-\delta}$ (YBCO) was the first synthesized HTSC with a T_c above 77 K. This ceramic superconductor is composed of Ytrium, Barium, Copper and Oxygen. The superconducting phase of YBCO material is crystallized in orthorhombic structure (Figure 2.2). The bottom and top Cu-O layers have oxygen only in the b-axis direction, forming Cu-O chains. All HTSCs have layered structure and the presence of CuO_2 layers plays a determinant role in their superconducting character. The current carriers only move along these planes, while the other components act as charge reserviors that regulate the charge density in the CuO_2 planes. In YBCO, as is shown Fig. 2.2, each unit cell contains two CuO_2 planes, separated by a plane of Ytrium atoms, and sandwiched by two BaO layers [3, 9, 15].

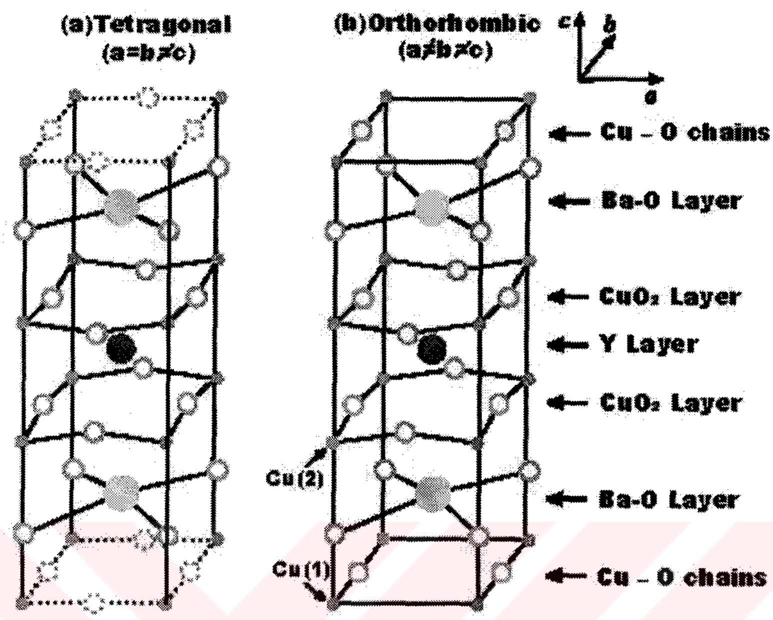

Figure 2.2: The unit cell of $YBa_2Cu_3O_{7-\delta}$, showing the different layers **(a)** Tetragonal (non-superconducting) **(b)** Orthorhombic (superconducting) [15].

The YBCO compound can be represented by two possible structures, one of them is tetragonal (a = b ≠ c), the other is orthorhombic (a ≠ b ≠ c). The unit cell parameters a, b, c depend strongly on the amount and distribution of oxygen in the structure. For low oxygen concentration ($\delta \leq 1$), the oxygen atoms are randomly dispersed in their four possible sites between Cu in the top and the bottom planes, leading to a tetragonal structure (Fig. 2.2(a)). However for $\delta \rightarrow 0$, oxygen atoms are ordered occupying only inter Cu sites along the b-axis of these planes and this leads to orthorhombic structure (Fig. 2.2(b)). In this case the Cu atoms form chains more than planes.

2.3 Critical Temperature and Zero Resistivity

One of the basic properties of superconductors is the disappearance of the resistance below a critical temperature T_c. The critical temperature of a superconducting material can be determined from the usual resistance versus temperature (*R-T*) measurements. *R-T* measurements show generally a metallic behavior from room temperature down to a certain temperature, and, then, a sharp drop in *R(T)* appears at the transition temperature. For $T < T_c$, the resistance becomes zero. It is now well established by means of modern equipments that, for $T < T_c$, the resistivity of superconductors is zero at least at the level of 10^{-24} $\Omega\cdot$cm.

2.4 Meissner Effect and Critical Current

Zero resistivity (infinite conductivity) is one of the most important characteristics of the superconducting state. However, the true nature of an superconducting state appears more clearly in the presence of the external magnetic field. The experiments performed in 1933 by Meissner and Ochsenfeld revealed that a superconductor completely expels sufficiently low magnetic flux when the sample is cooled below the critical temperature. This phenomenon is known as *Meissner* *effect* and such a flux exclusion is not observed in perfect conductors [9,10]. A schematic diagram which depicts the Meissner effect is shown in Figure 2.3 which also shows the difference between a superconductor and a perfect conductor.

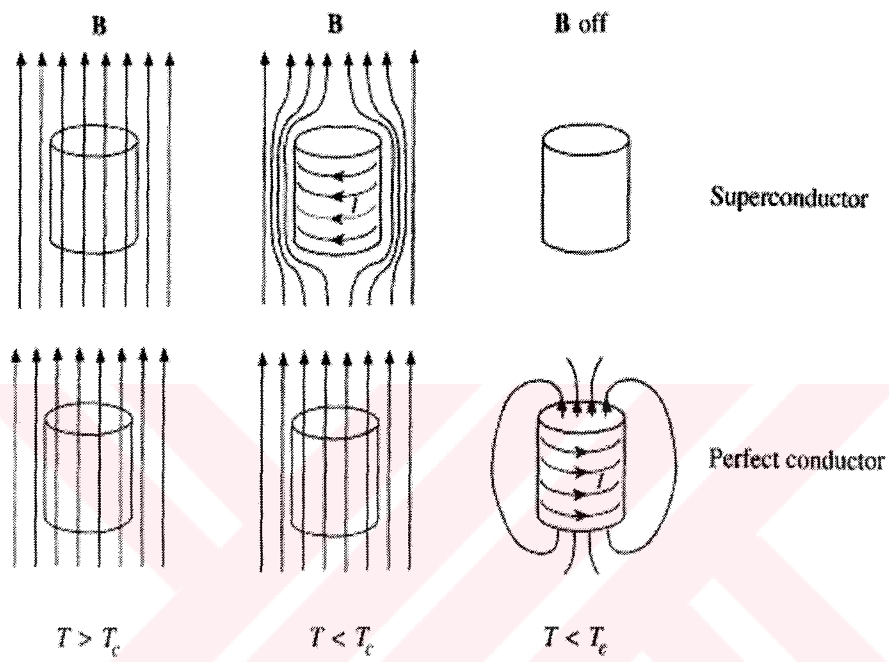

Figure 2.3 The Meissner effect. A superconductor cooled below its critical temperature expels all magnetic field lines from the bulk by setting up a surface current. A perfect conductor shows no Meissner effect.

2.5 Phenomenological Theories of Superconductivity

2.5.1 Two-Fluid Model and London's Theory

In 1934, Gorter and Casimir introduced a model concerning the thermodynamic treatment of the transition from normal to superconducting state, called *the two-fluid model of superconductivity*, by using the standard theory of phase transitions [2]. According to this model, the conduction electrons in the substance fall into two classes; superelectrons condensed in an ordered phase and normal electrons in a disordered noncondensed state. Although it has some successes, the two-fluid model has a restricted applicability: for instance, the Meissner effect can not be explained in the frame of this model. One year later, the two-fluid model was modified by F. London and H. London to explain the Meissner effect [3, 9, 10]. The London equations derived by using the conventional transport phenomena account for the Meissner effect. It was shown that the exclusion of the magnetic field from the sample is the natural result of the perfect diamagnetism. In addition, the London model predicts that the magnetic field penetrates into the sample to some extent. Thus, the magnetic flux is not expelled entirely from the superconductor, as was once thought, but there is a small region near the surface in which there is an appreciable field. This small region where the external magnetic field is penetrated is called the *London penetration depth* (λ). The general solution of the London equations gives that the magnetic field decays exponentially within the superconductor according to the relationship [3, 9, 18]

$$H(z) = H(0)\exp(-z / \lambda) \quad . \tag{1.1}$$

Here, $H(0)$ is the magnetic field at a distance $z = 0$ and is equal to the external magnetic field H parallel to the surface of the superconductor, and $H(z)$ is the local field at a distance of z inside the superconductor (Figure 2.4).

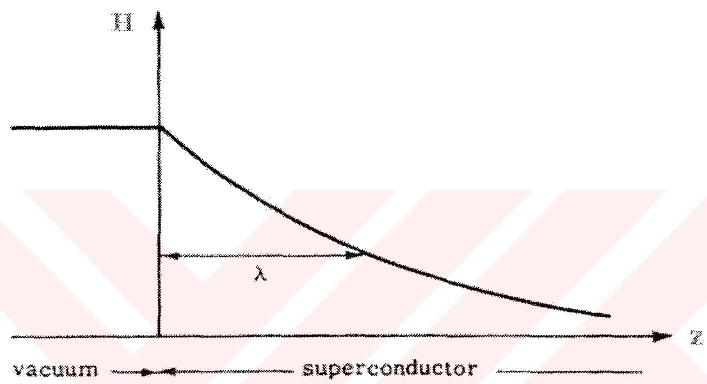

Figure 2.4 The London equation predicts that the external magnetic field decays exponentially in a superconductor occupying the region $z > 0$.

The London equations were generalized by Pippard [3,18] who suggested that the electrons in a pure bulk superconductor must act coherently over a characteristic length called the *coherence length* ξ_o. According to Pippard, only the electrons in the vicinity of the Fermi energy (E_F) contribute to superconductivity. Pippard's non-local theory was confirmed by the microscopic theories of superconductivity. [3,18]

2.5.2 Ginzburg-Landau Theory

In 1950, a new phenomenological theory of superconductivity was developed by V. Ginzburg and L. Landau, i.e., the GL theory, by considering the quantum effects [19]. London's theory did not take into account the quantum effects, hence, the GL theory is the first quantum mechanical treatment of superconductivity, which is an alternative to that of London's model. The GL theory is fairly successful in explaining many properties of superconductors, in particular, at temperatures near the critical temperatures. In GL theory, the behavior of superelectrons is described by an "effective wave function", $\Psi(r)$, which is considered as an order parameter so that $|\Psi|^2$ is assumed to be equal to the density of the superconducting electrons.

Furthermore, the superconducting state is more ordered than the normal one and the transition from one state to another is a second order phase transition. The GL theory was based on the Landau theory of second order phase transitions since the transition. The theory involves an expansion of the free energy in power series of $|\Psi|^2$, which is effectively small near the critical temperature.

The GL theory introduces an important dimensionless parameter, $\kappa = \lambda/\xi$ [the ratio of the penetration depth (λ) to the coherence length (ξ)], known as GL parameter,. Furthermore, a detailed analysis of the GL theory predicts a negative interphase boundary energy for $\kappa > 1/\sqrt{2}$ [3, 9, 18]. This indicate that this type of material will remain superconducting without exhibiting the Meissner effect, although the external magnetic field is greater than the thermodynamic critical field H_c where the superconductivity is destroyed. That is, the GL theory predicts the presence of an intermediate state which is a characteristics of another kind of superconductors called Type-II superconductors. This prediction is in good agreement with experiments. On the other hand, the GL theory gives a positive surface energy for $\kappa < 1/\sqrt{2}$ in another class of superconductors called Type-I superconductors, which have totally different electromagnetic properties when compared to Type-II ones [18].

For a special sample geometry, the relation between the supercurrent J_s and the order parameter $|\Psi|^2$ can be easily obtained by using the first and second GL equations: $J_s \sim |\Psi|^2$ [2, 17]. In other words, it is possible to determine how the transport current suppresses the order parameter. A similar calculation can be made to obtain a relationship between the external magnetic field H and order parameter $|\Psi|^2$. In this case, it can be shown that the $|\Psi|^2$ goes gradually to zero as H approaches a critical value [3, 18].

2.6 Type-I and Type-II Superconductors

Thirty pure metals exist which exhibit zero resistivity at low temperatures, and have the property of excluding magnetic fields from the interior of the superconductor. These metals are called Type-I superconductors and the superconductivity occurs below T_c and below a critical magnetic field strength. In addition, as mentioned in the previous section, a superconductor satisfying the condition $\kappa < 1/\sqrt{2}$ is also classified as Type-I [3, 9, 10, 18].

Type-I superconductors have zero electrical resistivity and zero internal magnetic field below T_c. The transition from superconducting to normal state in Type-I superconductors is fairly abrupt. The Type-I superconductors are useful for understanding superconductivity, but are of little practical value due to their low critical temperatures, small critical magnetic fields, and low current carrying capacity. Type-I superconductors are sometimes referred to as "soft" superconductors [3, 9, 10, 18].

Experimentally, it has been found that the magnetic and electric properties of metals, which show superconducting properties, differ from these of alloys and compounds. In order to distinguish them, Type-II superconductor term was introduced first by Abrikosov in 1957 [20, 21]. He proposed a phenomenological theory based on the GL theory to explain the magnetic properties of these materials. His theoretical treatments explained the origin of very high critical magnetic fields and also high critical currents in these materials.

The differences between Type-I and Type-II superconductors can be seen from magnetization measurements, i.e., *M-H* curves. The *M-H* curves of a long cylindrical samples of Type-I and Type-II superconductors which are placed in a magnetic field directed along the symmetry axis are shown schematically in Figure 2.5 [3, 9, 10, 18, 21]. It is seen from the *M-H* curve of a Type-I superconductor that, below its critical magnetic field H_c, the material is superconducting and the magnetic induction B in its interior is zero. When the external magnetic field H exceeds H_c, the superconductivity suddenly disappears and the material becomes normal. For a Type-II superconductor, the physical case is the same with that of Type-I superconductor when the external magnetic field is below the lower critical field H_{c1}: the material is in Meissner state and there is no

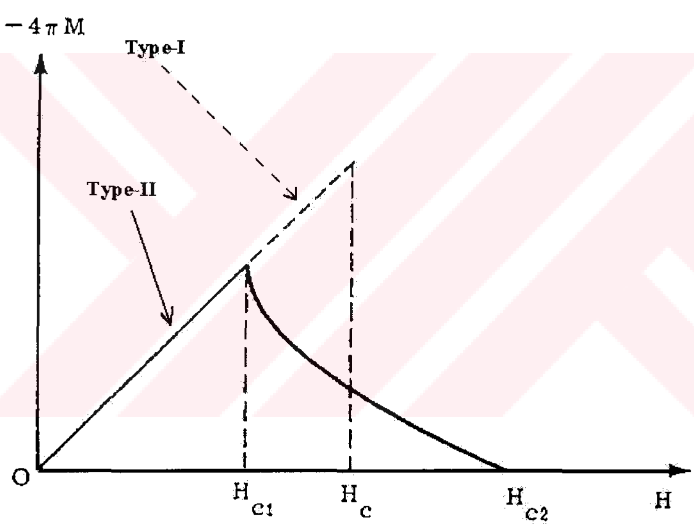

Figure 2.5 Magnetization curves for Type-I and Type-II superconductor.

flux penetration. However, for $H > H_{c1}$, the field lines penetrates into the sample in the form of quantized vortices, and an intermediate state consisting of normal and superconducting regions appears. As the external magnetic field becomes equal to the upper critical field H_{c2}, the bulk superconductivity disappears completely so that the flux lines are close to each other and their normal cores are come into contact [2, 8, 9, 17, 20].

Experiments show that the applied magnetic field penetrates into Type-II superconductors as quantized vortex filaments: each vortex carries one magnetic field flux quantum Φ_0. Penetration of vortices into the interior of a Type-II superconductor becomes thermodynamically favorable at $H > H_{c1}$. As the vortices enter into the superconductor, they arrange themselves at distances of about penetration depth λ from each other, so that, in the cross-section, they form a regular triangular lattice, as sketched in Figure 2.6 [3].

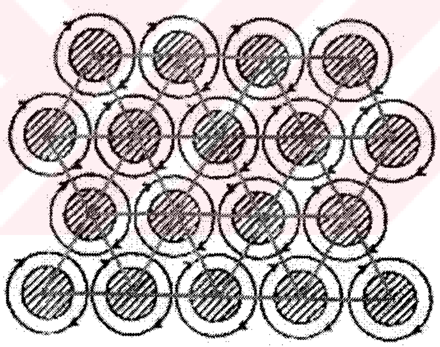

Figure 2.6 Regular triangular lattice formed by vortices in mixed state of a Type-II superconductor. Vortex cores (dashed areas) are in normal state.

Every filament (or vortex) has normal core in the normal state which can be approximated by a long thin cylinder with its axis parallel to the external magnetic field. The radius of the cylinder is of the order of the coherence length ξ. The direction of the supercurrent circulating around the core is such that the direction of the magnetic field generated by it coincides with that of the external field. In addition, the vortex current circulates within area of radius which is approximately equal to the penetration depth λ. For type-II superconductor, the size of this area must satisfy the condition of $\lambda >> \xi$ [18].

2.7 BCS Theory

The phenomenological theories summarized above are successful in explaining the thermodynamic and electromagnetic properties of Type-I and Type-II superconductors. A microscopic theory of superconductivity was developed by Bardeen, Cooper, and Schrieffer (BCS theory) in 1957 [22]. The BCS theory provided a deeper understanding of many physical properties of superconductors and explained also the other properties such as the acoustic attenuation, the superconducting tunneling etc., which can not be considered in the previous phenomenological theories. [18, 21]

According to BCS theory, the lattice vibrations in metal are active participanty in creating the superconducting state, and an extra interaction between electrons is maintained via quantized excitations of crystalline lattice, phonons. Under certain circumstances, this interaction takes the form of electron-electron attraction. If this interaction is stronger than the Coulomb repulsion between electrons, the electrons become effectively coupled, which gives rise to the superconducting state. Phonon mediated coupling of electrons leads to the well-known Cooper pairs.

The BCS theory agrees with the following experimental findings:

-The transition from the normal to superconducting state is a phase change of second order at a critical temperature T_c.

- T_c of crystals which contain different isotopes of the same element depends on the isotopic mass M. That is $T_c\sqrt{M}$ =constant.

-Most thermodynamic properties of a superconductor are found to vary as $e^{-\Delta/k_BT}$, indicating the existence of an energy gap Δ, or energy interval with no allowed energies in the energy spectrum (k_B is the Boltzmann constant) [3, 9, 10, 18, 20].

CHAPTER 3

GLASSY STATE RELAXATION AND FLUX DYNAMICS

3.1 Glassy State and Vortex Dynamics

The electrical and magnetic properties of HTSCs are fairly unusual and still subject of intense research. It was observed that there is a fast relaxation in magnetization measurements (*M-H* curves) which is mainly originated from their higher operating temperatures and low pinning energy due to short coherence lengths [23]. Many theoretical models, such as the classical Anderson-Kim flux creep model [24], vortex glass [25], power law [26], vortex lattice melting [27], and collective-creep model [28] have been proposed to explain the anomalous time decay of magnetization observed in HTSCs. In addition to *M-H* curve measurements, recent studies showed that there are remarkable time effects in transport measurements, which can be observed via both slow and fast measurement techniques [5, 6]. The superconducting glass model [29], modified flux flow and resistive weak-link models [30], two-kind-of flux creep model [31] have been developed in order to explain the unusual time effects observed in these studies.

Some magnetic properties of HTSCs, which cannot be explained within the framework of the conventional flux creep theory, are interpreted in terms of the field/current induced glassy effect. Such an effect in HTSCs reminding the spin glasses was first reported by Müller *et al.* [32] and, then, reported in a bulk superconducting $Y_1Ba_2Cu_2O_{7-\delta}$ (YBCO) Karimov and Kikin [29]. Recently, the fast transport measurements performed by Henderson *et al.* [7] and Xiao *et al.* [33] have confirmed such a glassy relaxation in single crystal samples of 2H-$NbSe_2$ and Fe-doped 2H-$NbSe_2$. Indeed, the flux creep picture and the other theories can not solely explain the transition to a state with a vanishingly small voltage.

In the glassy state relaxation, it is assumed that there are several energy states for the moving entities with a hierarchy of barriers. Within this description, it is assumed that the energy difference between the neighboring barriers (F_o) is small, while the difference between the more distant barriers (P_o) is higher [29]. Such an energy landscape leads to the concept of the superconducting glass model. A schematic diagram showing this is given in Figure 3.1. Due to the external force or thermal activation, the vortices can easily overcome the neighboring barriers, but may fall in a deeper barrier. Bundle of vortices remaining at the bottom of deeper barriers can not overcome the barriers and give no contribution to the measured voltage.

During the time evolution of the sample voltage, the decrease in voltage can be correlated with the decrease in the number of the flux lines which lose their capability of motion. This implies that some of the vortices are pinned by the pinning centers in an inhomogeneous distribution of the energy landscape.

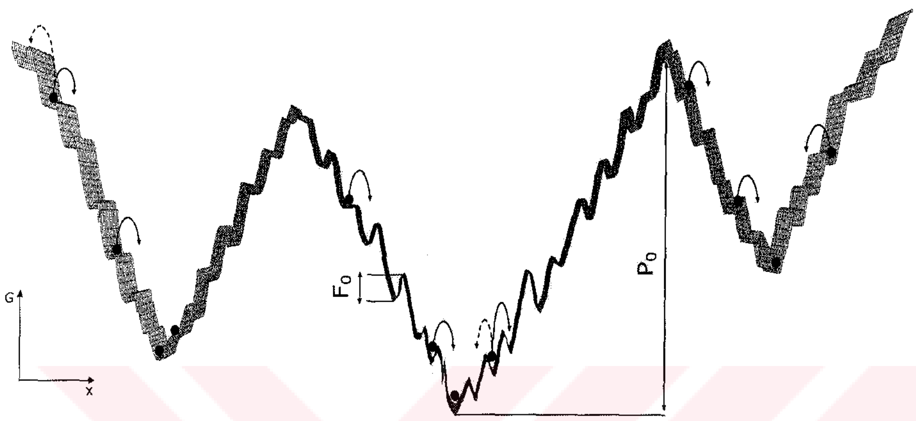

Figure 3.1 Energy landscape of a superconducting glassy system, free energy (G) vs. position (x) of vortices. The neighboring potential barriers are denoted as F_0, whereas, P_0 is the effective (deep) potential barrier [29].

The relaxation of remanent magnetic moment in spin glasses is described by a stretched exponential form [29]:

$$M(t) = M_o \exp\left[(-C\frac{t}{\tau_o})^{1-n} \Big/ 1-n \right] \quad , \qquad (3.1)$$

where M_0 is the magnetic moment at time $t = 0$, C is a constant, n is a temperature dependent parameter, and τ_0 is a characteristic time and depends on the external magnetic field, transport current and temperature. Equation.3.1 shows that the total magnetic moment at any time is defined by the degree of ordering of individual magnetic moments. A similar case is encountered for the vortices in a superconductor passing into a state of minimum energy. Thus, a minimization process brings naturally occupation of vortices in a minimum energy state within the corresponding energy landscape. As the time passes, the superconducting order parameter may enhance over the whole sample, which leads to a decrease in the sample voltage.

Equation.3.1 can be transformed into an empirical relation by taking $C = 1$ and $n = 0$, and can be rewritten in a more simple form [29]:

$$V(t) - V(t=0) = \exp(-t/\tau_o) \tag{3.2}$$

Here V is the sample voltage and the other parameters have the same meanings as given above. Equation.3.2 gives fairly reasonable insight on about the decay of sample voltage below T_c [29, 33]. However, it should be emphasized that one of the most important requirements to get a glassy state is to switch off the power supply, which generates the transport current (or magnetic field), or reduce it to a given finite value. Thus, it becomes possible to create a quenching state which is unstable in time, and the measurable time independent parameters of the system become remarkably time dependent.

CHAPTER 4

SAMPLE PREPARATION AND EXPERIMENTAL SET UP

4.1 Sample Preparation

The polycrystalline bulk $Y_1Ba_2Cu_3O_{7-\delta}$ (YBCO) samples were prepared from high purity powders of Y_2O_3, $BaCO_3$, and CuO (Algrich Co.). All the powders are of %99.99 purity. The powders were weighted in the stoichimetric proportions by using an electronic balance (Sartorius CP2245). They were mixed and grounded approximately 1 hour in agate mortar in order to obtain an homogenous mixture. The mixed powder was put in alimuna (Al_2O_3) crucible for calcination. The calcination process was carried out at 930 °C for a duration of 12 hours in a microprocessor controlled tube furnace (Carbolite CTF 12/100/90). After the calcination, the powders were regrounded and pestled in an agate mortar approximately 1 hour. Then, the powder was pressed under 10 tons of pressure for 5 minutes by using a press [Lightpath Optical (UK) LTD]. Thus, the powder was pelletized to obtain a disc shape pellet with a diameter of 10 mm. Figure 4.1 shows the furnace set-up where the YBCO samples are annealed.

In order to obtain the desired phase these pellets were put again into the furnace for sintering and were annealed under oxygen (O_2) atmosphere with a pressure of

~ 1 atm at 950 °C for a duration of 12 hours. The pellets were cooled down to the room temperature with a low cooling rate of 1 °C/min. The processes including grounding and sintering outlined above was repeated twice to raise the quality of the samples.

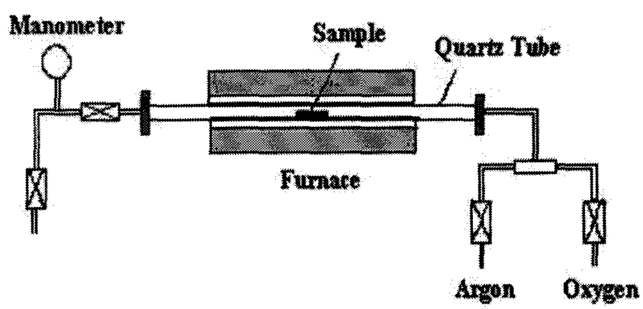

Figure 4.1 Furnace set-up where the samples were annealed [34].

At final step, to guarantee the sufficient O_2 uptake, the samples were annealed at 550 °C for 12 hours at O_2 atmosphere, then, the samples were cooled down to room temperature with a rate of 1 °C/min. Following this process, the samples having diameter of 10 mm and thickness of ~ 1.8 mm were obtained.

The YBCO pellet was cut by using a diamond saw in the form of rectangular bars, which were then carefully shaped in the form of rectangular prism with typical dimensions of length ℓ = 4 mm, width w = 0.1 mm, and thickness d = 0.2 mm. Such low dimensions are necessary to eliminate any possible Joule heating effects on the current leads. Copper wires with a diameter of 0.5 mm for current and voltage leads were attached to the sample by using good quality silver paint (Electroday, 1415). After making the electrical contacts, the sample was placed carefully into a closed cycle refrigerator [Oxford instruments, (OI) CCC1104]. In order to eliminate the resistance of the copper wires attached to the sample, the conventional four point method was used for the transport measurements.

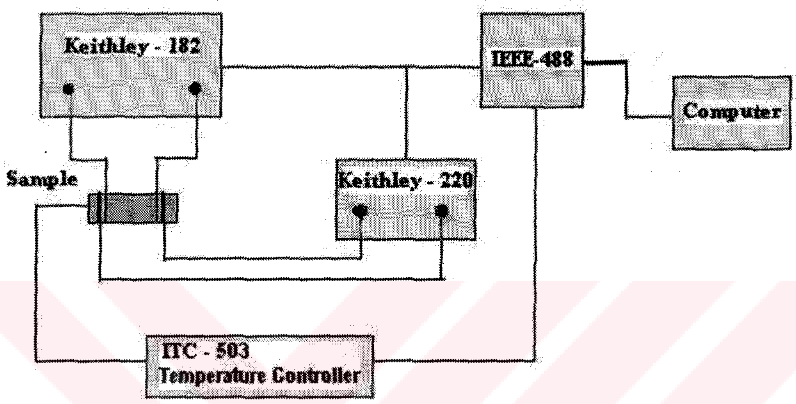

Figure 4.2 Block diagram of the experimental set-up used for transport measurements [33].

4.2 Measurement Set-Up

A block diagram of the measurement set-up is given in Figure 4.2. All measurements were carried out under PC control via an IEEE-488 interface card. A temperature stability better than 10 mK was maintained during the measurements (OI, ITC-503 temperature controller). The temperature was measured by using a calibrated 27 Ohm-Rhodium-Iron thermocouple (OI, Calibration number 31202). Keithley-182 (nanovoltmeter) with a resolution of 1 nV and Keithley 220 (current source) were used in measuring the sample voltage and supplying the current, respectively. The nanovoltmeter was triggered for a maximum of 61/2 digits, and its buffer was read directly within the integration time of 100 ms in order not to cause any artificial effect. The measured voltage is the average value of 5 readings for each data point.

In order to determine the current carrying capacity of the samples, the current-voltage (*I-V*) characteristics were measured at temperatures near the critical temperature of the samples. The critical current density of our YBCO samples whose results are presented in this study is of order of ~25 A / cm^2 at $T = 88$ K determined by using the 1 μV / cm criterion.

In this study, the time evolution of voltage (V - t curves) was measured at zero applied magnetic field by applying dc and bidirectional square wave current with long period (P) at different amplitudes to the sample. For our purpose, the current source (Keithley - 220) and nanovoltmeter (Keithley - 182) are suitable to produce bidirectional square wave currents with long periods and to read low voltage levels with a large precision. Just after the current is applied to the sample, we start to measure the developing voltage along the sample as a function of time. Thus, it becomes possible to monitor all the details of the time evolution of the sample voltage, including the transient effects. To create a quenched state, the dc current (I_1) was interrupted or reduced to a finite value (I_2). In addition, during the course of experiments, the bidirectional current was switched to dc currents to assess their different effects in the final stage of some of the measurements.

CHAPTER 5

EXPERIMENTAL RESULTS

5.1 Resistivity vs Temperature Measurements

A typical example for the resistivity vs temperature (ρ - T) curves of YBCO is given in Fig.5.1. The ρ - T curve in the normal state above T_c shows a metallic behavior: The resistance decreases approximately linearly with decreasing temperature until the superconducting transition occurs at T_c.

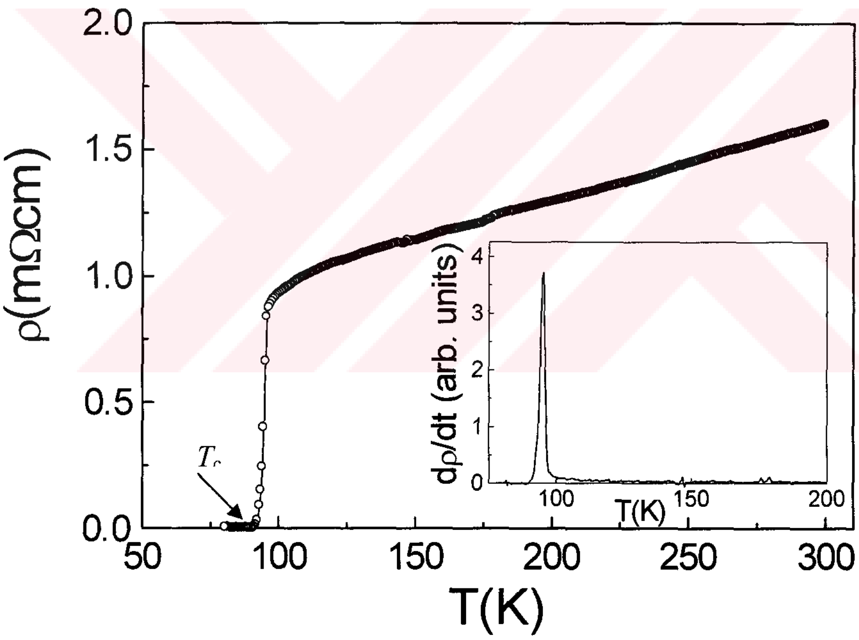

Figure 5.1 The resistivity of bulk polycrystalline YBCO sample as a function of temperature. The inset shows the derivative of resistivity with respect to temperature.

The derivative of the resistivity with respect to temperature is also given in the inset of Fig.5.1. The critical temperature T_c of the sample at zero magnetic field is measured to be ~ 92 K, which is consistent with those given in the literature for polycrystalline $YBa_2Cu_3O_{7-\delta}$ with high oxygen content (i.e., $\delta \cong 0.1$).

5.2 Current-Induced Organization at Different Currents and Temperatures

5.2.1 Formation of Quenched State for $I_1 > I_2$ at Different Temperatures

One of the best ways to observe the time effects induced by the transport current is to record the sample voltage continuously as a function of time, i.e., to measure the V - t curves. Thus, all dynamic changes including the transient effects can be monitored. During the time evolution of the sample voltage, the transport current (I_1) can be interrupted or reduced to a finite value (I_2) so that a quenched state which is reminiscent of the glassy state can be obtained. Indeed, to create a glassy state, one of the requirements is to interrupt the power supply which generates the transport current (or the external magnetic field) or to reduce the transport current (or the external magnetic field) to a lower value. For this purpose, in our measurements, a dc driving current, I_1, was applied to the sample and maintained for 53 s to achieve a steady state. Then, the current was reduced from I_1 to a lower value, I_2, during course of the measurement, and this value kept at rest of the relaxation process, i.e., up to 120 s. In the mean time, the sample voltage was recorded continuously.

Figure 5.2(a) shows a set of typical V - t curves measured at T = 87 K for I_1 = 30 mA, and I_2 = 0, 2, 4, 6, 8, 10, 12, 14, 16, 18, and 20 mA. It is seen, before reducing the driving current from I_1 to I_2, that the sample voltage evolves in two stages : In first stage, a sharp increase in sample voltage is observed for $t \leq 10$ s, and, then, in second stage, the current becomes approximately constant, which implies that a steady state develops in the sample. After reducing the

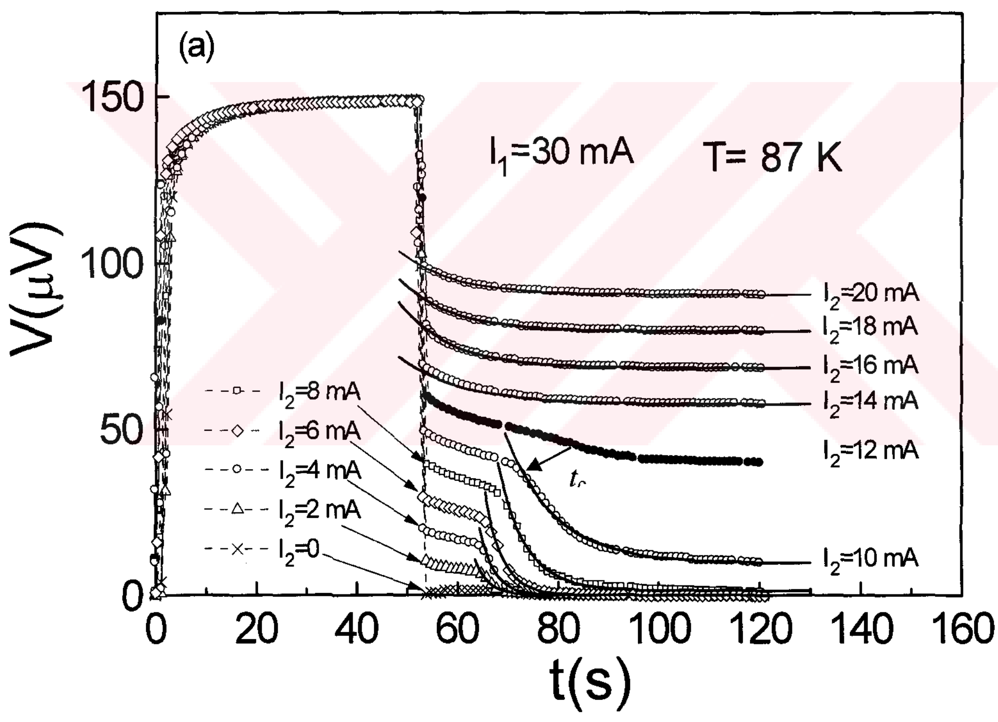

Figure 5.2(a) Time evolution of the V - t curves measured at T = 87 K for I_1 = 30 mA, and I_2 = 0, 2, 4, 6, 8, 10, 12, 14, 16, 18, and 20 mA. The initial current I_1= 30 mA was applied for 53 s, it is then reduced to I_2 and left on the sample. The dashed lines through the data points are guides for the eye and the solid lines are the calculated curves defined by Eq. 3.2.

from I_1 to I_2, the sample voltage exhibits several different behaviors depending on the magnitude of the current I_2. When $I_2 = 0$, the sample voltage becomes zero and no trace of relaxation effect is observed. This indicates that ***(i)*** there is no residual voltage on the sample to be relaxed within the time response of the experimental set-up, and ***(ii)*** the observed voltage decays observed for $I_2 > 0$ are physical, which are not originated from the limitations of the experimental set-up. The *V-t* curves measured in the current range 2 mA $\leq I_2 \leq$ 10 mA evolve in the form of voltage decays with two stages. A smooth transition which follows the first

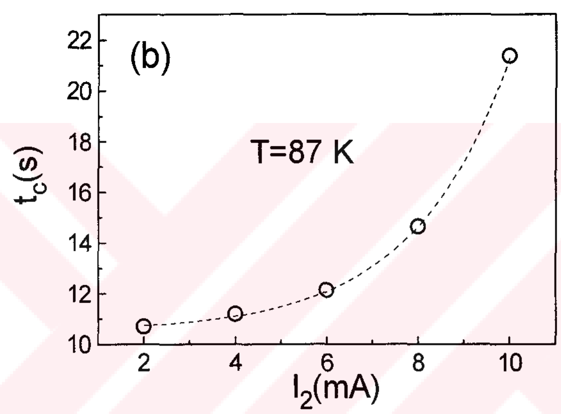

Figure 5.2(b) Variation of the critical time t_c with the current I_2. The dashed line is a guide for eye.

voltage decay develops after a certain critical time (t_c) value which depends on the magnitude of I_2. The t_c is the elapsed time from the beginning of the voltage decay to the onset of the transition time. The variation of t_c with I_2 is plotted in Fig. 5.2(b): t_c increases non linearly with increasing of I_2. For I_2 = 2, 4, 6, and 8 mA, the smooth transition results in a superconducting state since the measured voltage is zero. The evolution of the superconducting state occurs in shorter times for low values of I_2 as compared to that of observed for higher I_2 values. Although a transition evolving to the superconducting state is observed in the V - t curves obtained for I_2 = 10 and 12 mA,, the zero resistance state is not yet established for these current values (Fig. 5.2(a)). On the other hand, the behavior of the V - t curve corresponding to I_2 = 12 mA is somewhat different from the V - t curves for $I_2 \leq 10$ mA. In this V - t curve, a transition to superconducting state is not so prominent as for the curves with $I_2 \leq 10$ mA. We propose that the current I_2 = 12 mA separates the low and high current regions. Because, the V - t curves corresponding to $I_2 > 12$ mA decay over time without showing any transition during the measurement.

The solid lines in Fig. 5.2(a) represent the curves calculated by using Eq.3.2. There is a reasonable agreement between the experimental data and the calculated curves in the range $t > t_c$.

In order to assess the effect of temperature on the evolution of the V - t curves, similar measurements at 86.5 K were carried out by applying the same experimental procedure described in Fig.5.2(a). The reason of choosing a temperature which is very close to that in Fig.5.2(a) is that the evolution of V - t curves are very sensitive to small changes in temperature. The measurements were repeated for the same current values of I_1 = 30 mA and I_2 = 0, 2, 4, 6, 8, 10, 12, 14, 16, 18, and 20 mA. The experimental data are plotted in Figure 5.3(a). The inset of Fig.5.3(a) shows the $V - t$ curves for I_2 = 18 and 20 mA with I_1 = 30 mA. Here, differently, the initial current I_1 is left on the sample for the first 71 s.

It is seen from the main panel of Fig. 5.3(a) that, as the magnitude of current is reduced from I_1 = 30 mA to I_2 at t = 53 s, the sample voltage drops abruptly, and, then, decays nonlinearly up to a certain time t_c (the critical time) which depends on the magnitude of I_2. The variation of critical time t_c with I_2 as extracted from

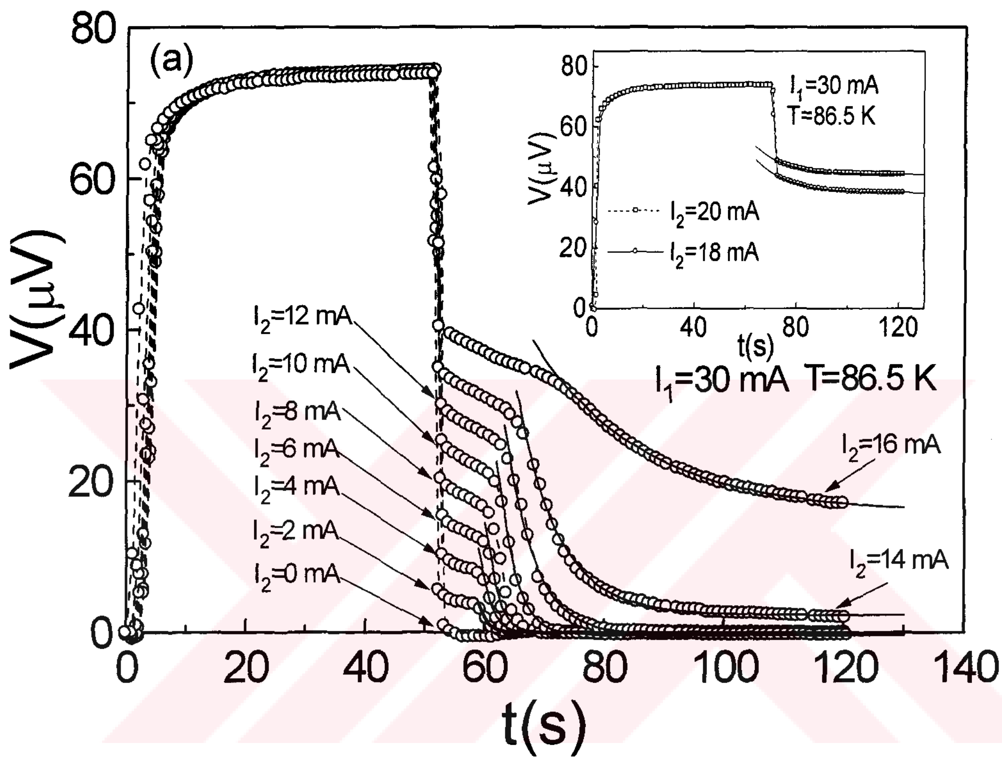

Figure 5.3(a) Time evolution of the V - t curves measured at T = 86.5 K for I_1 = 30 mA, and I_2 = 0, 2, 4, 6, 8, 10, 12, 14, 16, 18, and 20 mA. The initial current I_1 = 30 mA was applied on the sample for 53 s, it is then reduced to I_2 and left on the sample. The inset shows the V-t curves measured at the current values I_2 = 18 and 20 mA, respectively. The reduction from I_1 to I_2 was carried out at t = 71 s of the time evolution. The dashed lines are a guide for the eye and the solid lines are the calculated curves defined by Eq. 3.2.

Fig. 5.3(a) is illustrated in Fig. 5.3(b). For $t > t_c$, a transition follows the initial smooth decay evolving to lower voltage values. For the current values of I_2 = 2, 4, 6, 8, 10, and 12 mA, the transition results in a superconducting state, whereas, for I_2 = 14 and 16 mA, the smooth voltage decays together with transitions do not result in a superconducting state.

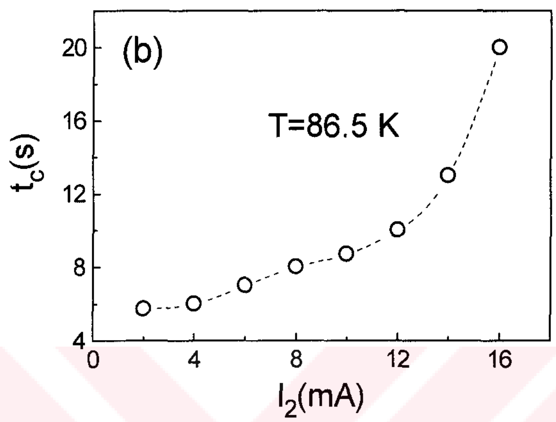

Figure 5.3(b) Variation of the critical time t_c with current I_2. The dashed line is a guide for eye.

A comparison between Fig.5.2(a) and Fig.5.3(a) shows that, in addition to similarities, there are also some differences. For instance, the transition at I_2 = 12 mA in Fig. 5.3(a) results in a superconducting state, whereas, for the same current value in Fig.5.2(a), such a behavior evolving to zero resistance state is not seen. We believe that this behavior is due to the change of temperature. On the other hand, the dependence of t_c on the current I_2 (Fig. 5.2(b) and Fig. 5.3(b)) demonstrates these differences well and reveals the effect of the temperature on the evolution of the V - t curves. The comparison of t_c values obtained at different temperatures shows that both the evolution of voltage decays and the width of the transitions depend strongly on the temperature, which implies the lower the temperature the lower the critical time. As can be seen from the inset of Fig. 5.3(a), at the higher current values of 18 and 20 mA, only voltage decays without a transition to superconducting state are observed.

5.2.2 Correlation between Quenched State and the Magnitude of the Transport Current I_1

To investigate the influence of the magnitude of driving current I_1 on the evolution of the V - t curves, the current I_1 was reduced from 30 mA to 20 mA and the V - t curve measurements were repeated for I_2 = 0, 2, 4, 6, 8, and 10 mA at T = 87 K. The data are represented in Figure 5.4. A comparison of Fig. 5.2(a) and Fig. 5.4 shows that there is a similarity between the corresponding V - t curves. The response of the sample to the reduction of I_1 = 20 mA to I_2 shows nearly the same behavior as compared to that of observed in Fig. 5.2(a), i.e., the time evolution of the sample voltage occurs in two stages. However, a careful examination reveals that there are remarkable differences between the V - t curves presented in Figs. 5.2(a) and 5.4. First of all, just after the current I_1 is reduced to I_2, the sample voltage decays and evolves to superconducting state within shorter times. This can be easily understood from the inset of Fig.5.4 which shows shorter critical time values as compared to those Fig. 5.2(b). For instance, the t_c values corresponding to I_2 = 8 mA in Fig. 5.2(a) and Fig. 5.4 are 15 s and 9 s, respectively. This emphasizes that, at low values of the initial current I_1, the smooth transitions are observed within shorter times.

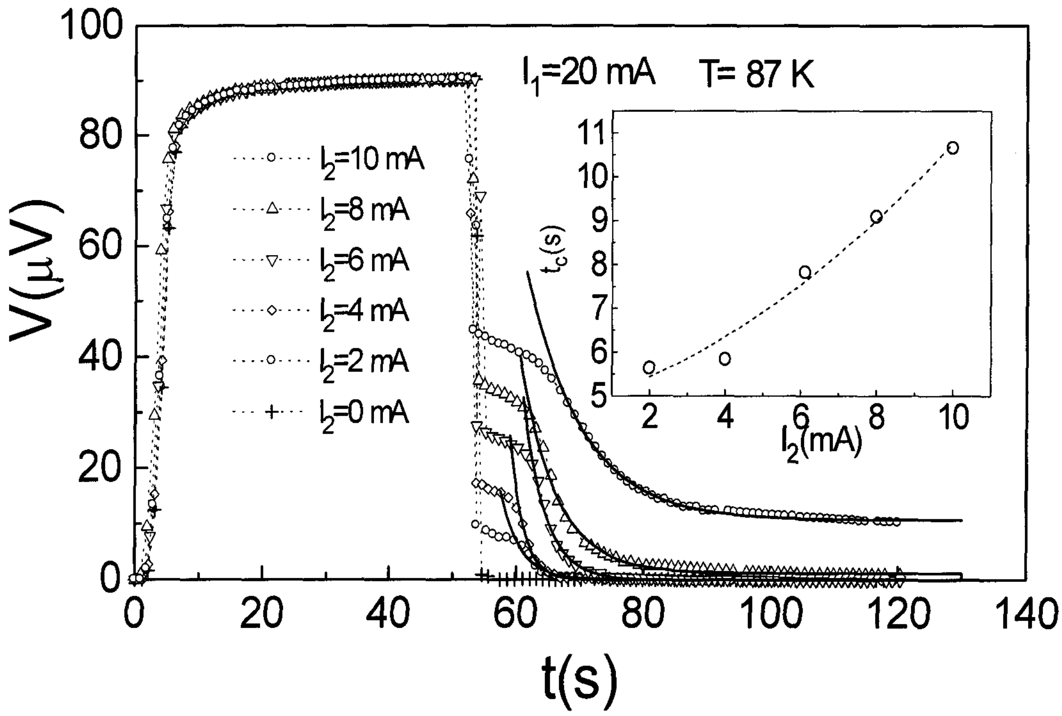

Figure 5.4 Time evolution of the V - t curves measured at T = 87 K for I_1 = 20 mA, and I_2 = 0, 2, 4, 6, 8 and 10 mA. The initial current I_1 = 20 mA was applied for 53 s, it is then reduced to I_2 and left on the sample. The inset shows the variation of the critical time t_c with the current I_2. The dashed lines through the data points are guides for the eye and the solid lines are the calculated curves defined by Eq. 3.2.

5.2.3 Evolution of $V - t$ curves for $I_1 < I_2$ and Observation of Residual Voltage V_r

In the experiments described above, the initial driving current I_1 was applied to the sample for a while and then reduced to a lower value of I_2, i.e., $I_1 > I_2$. In order to investigate the effect of the driving current magnitude on the evaluation of V - t curves, experiments were performed under the condition $I_1 < I_2$. That is, a current

I_1 smaller than I_2 was selected and was left on the sample for waiting time of 53 s. Then, it was increased from I_1 to I_2. We observed that, in all experiments, the waiting time between the two successive experiments influences the evolution of the V - t curves. Therefore, the experimental set-up was programmed such that the time interval between two successive experiments is 10 s.

Figures 5.5(a)-5.5(e) show the time evolution of the typical V - t curves at T = 87 K for selected values of I_1 with I_2 = 20 mA ($I_1 < I_2$). The V - t curve measured for I_1 = 10 mA and I_2 = 20 mA evolves in three stages, before increasing the driving current from I_1 to I_2. In the first stage, initially, any measurable voltage response is not observed within a delay time of ~ 10 s. In second stage, the sample voltage starts growing up non-linearly. Finally, in third stage, after ~ 30 s, the voltage becomes time independent, i.e., the sample reaches nearly a steady state. At around t = 53 s, the driving current I_1 = 10 mA was abruptly increased to I_2 = 20 mA. The response reflects itself initially as a sharp jump in voltage and then a steady state is observed at times up to 120 s.

Figure 5.5(b) shows the V - t curve measured at 87 K for I_1 = 12 mA and I_2 = 20 mA 10 s later than that in Fig. 5.5(a). It is seen that there is a marked difference between the V - t curves presented in Fig. 5.5(a) and Fig. 5.5(b). In Fig. 5.5(b), the voltage reaches a steady state in one stage. Here, it seems that the V - t curve begins from a residual voltage value. Abrupt increase in the driving current from 12 to 20 mA leads to the usual response as shown in Figs. 5.5(a) to 5.5(e).

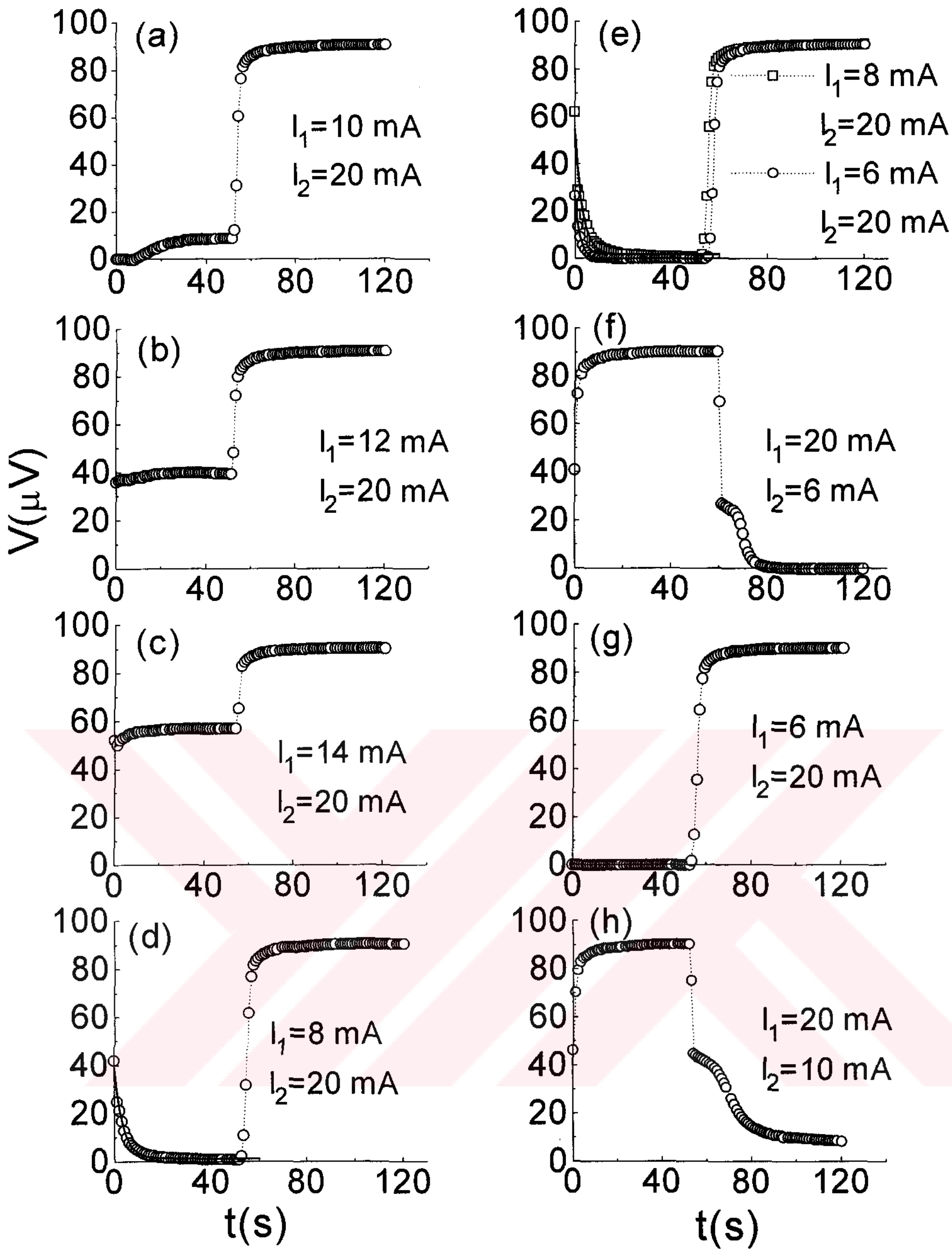

Figure 5.5 Time evolution of the V - t curves measured successively at T = 87 K as a function of different sequences of the currents I_1 and I_2 as given in each panel. The time between two successive V - t curves is 10 s. The dashed line through data points is a guide to the eye and the solid line in panels (d), (e), and (j) is the calculated curves by using Eq.3.2.

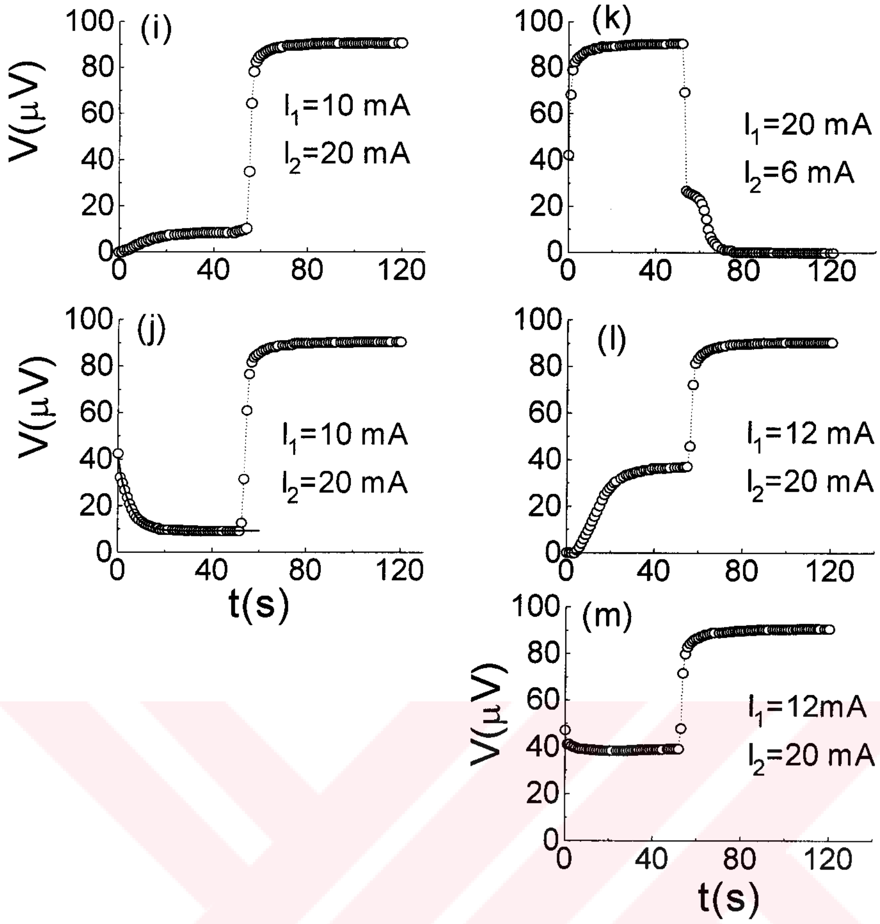

(Continued)

We repeated the experiment, by increasing the current I_1 from 12 to 14 mA, and keeping the other experimental parameters the same. The evolution of the V - t curve is illustrated in Fig. 5.5(c). A small increase in I_1 does not cause any dramatic change in the $V-t$ curve and a behavior similar to that in Fig. 5.5(b) was observed.

In the next measurement, the driving current I_1 is lowered to 8 mA (Fig. 5. 5(d)). As can be seen, the V - t curve in this figure exhibits a response which is quite different from the other ones presented above. At the beginning of the relaxation process, a large residual voltage $V_r \sim 45$ μV was measured, which is similar to those in Fig. 5.5(b) and Fig. 5.5(c). Within very short time, an quick drop in V_r occurs followed by a smooth voltage decay evolving to zero resistance state which develops up to 53 s. After this time value, increasing of the driving current from 8 mA to 20 mA leads to the evolution of an usual V - t curve with two-stage.

To confirm the soundness of the data represented in Fig. 5.5(d), this interesting measurement was repeated under the same experimental conditions but for $I_1 = 6$ mA (Fig. 5. 5(e)). At the beginning of the relaxation process, the sample voltage decays rapidly and reaches the zero resistance state earlier than that of the V - t curve measured for $I_1 = 8$ mA.

In order to remove the large residual voltage trapped inside the sample, we return back to our usual experiments carriet out under the condition $I_1 > I_2$. The driving current I_1 was increased to 20 mA and I_2 was reduced to 6 mA. The data thus obtained are illustrated in Fig. 5.5(f). It is seen that, although the V - t curve begins with a residual voltage, it exhibits a similar behavior with the ones presented in Figs.5.2(a), 5.3(a), and 5.4. We note that, at long times of the relaxation process, the sample voltage becomes exactly zero and the zero resistance state is fully established. In order to test whether the residual voltage on the sample is physical or not, the experiment under conditions described in Fig.

5.5(d) and Fig. 5.5(e) (i.e., I_1 = 6 mA and I_2 = 20 mA) were repeated. The V - t curve is plotted in Fig. 5.5(g) which shows that the initial sample voltage now became zero up to the time where the current I_1 was changed to I_2. That is, there was no residual voltage to be relaxed. We suggest that the experimental procedure considered in Fig. 5.5(f) removes the residual voltage trapped inside the sample.

To give a further support for this physical picture and also the suggestion that we pointed out above, we continued to repeat the experiments at T = 87 K. Fig. 5.5(h) depicts the V - t curve obtained for the currents I_1 = 20 and I_2 = 10 mA. A behavior similar to that in Fig. 5.5(f) was observed. The reduction of current at around 53 s leads to a voltage decay and smooth transition evolving to smaller voltage values, however, the superconducting state is not reached.. We assume that this is the first step to remove the residual voltage in the sample.

In the next step, the V - t curve was measured for the currents of I_1 = 10 and I_2 = 20 mA. Fig. 5.5(i) depicts the evolution of this V - t curve. As in the case of Fig. 5.5(a), it is seen that the V - t curve evolves in three stages from the beginning of the relaxation effect to time t = 53 s. Beyond this time, an usual response evolves as the current is increased from 10 to 20 mA. Without changing the experimental conditions, this experiment was repeated for the same current values. As can be seen from Fig. 5.5(j), a large residual voltage which decays with time appears again. Note also that the relaxation process from the beginning of the measurement to t = 53 s does not result in zero resistance state. We suggest that this finding is closely related to the magnitude of the driving current, because, the superconducting state was reached in the evolution of the V - t curves measured for the lower values (8 and 6 mA) of I_1 , as demonstrated in Figs. 5.5(d) and 5.5(e).

We now know how to remove the residual voltage (V_r) trapped inside the sample. To do this, it is sufficient to follow the experimental route outlined in Fig. 5.5(f). The driving current I_1 was first increased to 20 mA and then switched to 6 mA. Thus, at long times of the relaxation process, the sample voltage becomes essentially zero (see Fig. 5.5(k)).

The V - t curve illustrated in Fig. 5.5(k) show again the process to remove V_r. In Fig. 5.5(l), as one would expect, any residual voltage is not observed in the V - t curve measured for I_1 = 12 mA and I_2 = 20 mA. However, the $V - t$ curve measured just after the one shown in Fig. 5.5(l) shows that the residual voltage reappears (Fig. 5.5(m)).

Finally, we conclude that (*i*) the residual voltage can be re-stored provided that the condition $I_1 < I_2$ is satisfied, and (*ii*) the magnitude of the driving current and the sequence between I_1 and I_2 influence substantially on the evolution of the V - t curves.

5.3 Influence of Bi-directional Square Wave (BSW) Transport Current on the Evolution of $V - t$ Curves

In this section, we investigated the time evolution of voltage (V - t curves) at low dissipation levels for different types of transport currents, such as dc current and bidirectional square wave current with long periods, in YBCO material. The measurements were carried out as a function of temperature (T), current (I), and the period (P) of bidirectional square wave current on both short and moderate time scales at zero field.

5.3.1 Time Evolution of the V - t curves for BSW current with Long Periods and Different Amplitudes

Figures 5.6(a) to 5.6(c) show the long time evolution of the sample voltage measured at T = 88.5 K for a bi-directional square wave (BSW) current with a period (P) of 86 s and amplitude of 16, 18 and 20 mA, respectively. The upper panel in each figure shows the time variation of the driving BSW current. To compare the effect of BSW current on the V - t curve with that of dc current, at around 1050 s, the BSW current was switched to positive dc current corresponding to the amplitude of BSW (i.e., +16, +18, and +20 mA) for the rest of the relaxation process. As is seen from Fig. 5.6(a), at low amplitudes of BSW current, the response shows an asymmetric behavior (with respect to the zero voltage). As the amplitude of BSW is increased, the amplitude of the response gradually grows up and the asymmetric behavior in V - t curves disappears progressively (Figs. 5.6(b) and 5.6(c)). That is, along with increase in amplitude of the BSW current, the lineshape of the V - t curves improves and exhibits more regular behavior. Another experimental observation is the significant relaxation effects which manifest themselves as a decrease or increase in the absolute value of the sample voltage, when the BSW current remains constant, i.e, positive or negative. In these figures, the voltage decreases with time in every half-period which the BSW current is positive, except the one at the beginning. However, for the negative part of the driving current, a nonlinear negative increase in voltage is observed, which implies that the dissipation is enhanced. In addition, we note that the relaxation effects in voltage corresponding to the time intervals where the driving current remains constant decreases, as the amplitude of the BSW current increases.

On the other hand, when the BSW current was switched to a positive dc current, the repetitive behavior of the corresponding V - t curves disappears, as would be expected, and a dynamic change reflecting the influence of the magnitude of dc current develops on the sample. It is seen from Figs.5.6(a) to 5.6(c) that there is a relative decrease in the amplitude of the measured voltage which depends on the magnitude of the dc current. In addition, the sample voltage reflects directly the changes in BSW drive. In another words, the voltage follows the current and, thus, any phase difference between the BSW drive and the sample voltage does not occur.

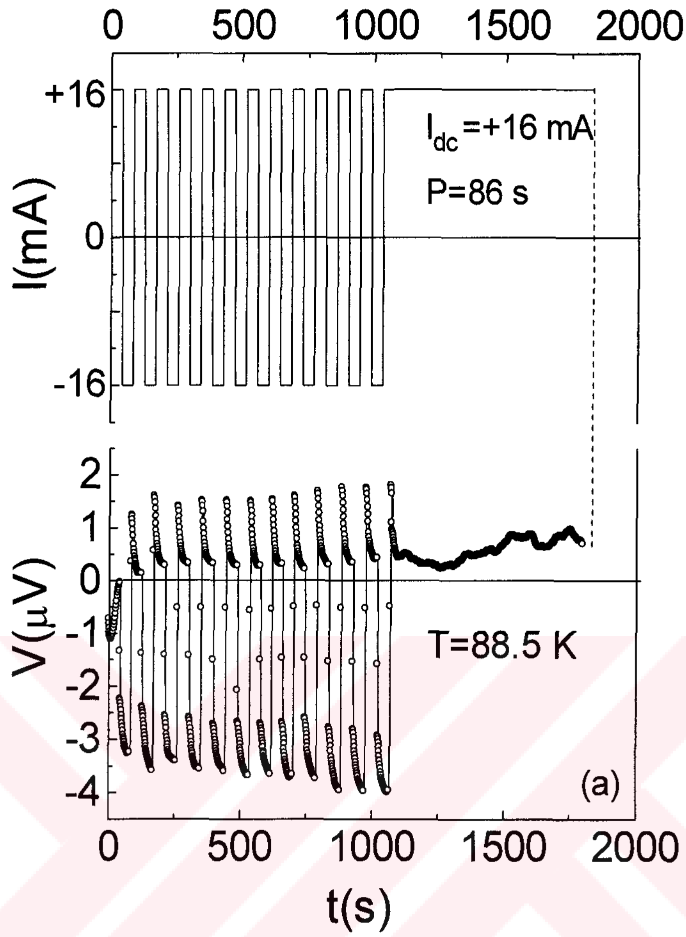

Figure 5.6(a) Long time evolution of the voltage measured at T = 88.5 K for a bi-directional symmetric square wave (BSW) current with an amplitude of 16 mA and period of 86 s. The upper panel shows the time variation of the driving BSW current. At t = 1050 s, the BSW drive was switched to + 16 mA dc current for the rest of the relaxation process.

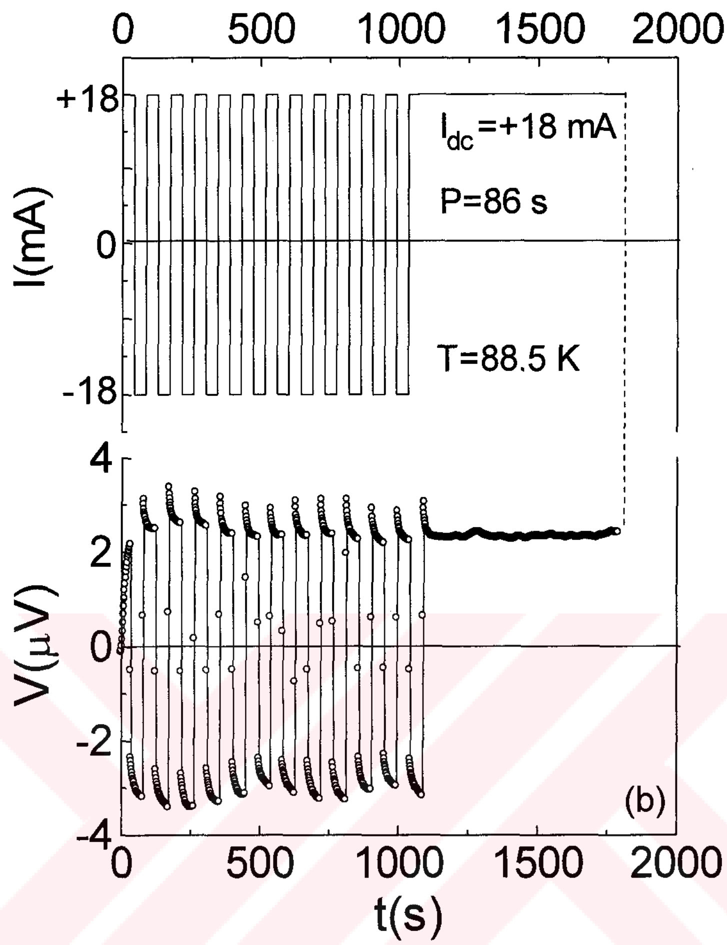

Figure 5.6(b) Long time evolution of the voltage measured at T = 88.5 K for a bi-directional symmetric square wave (BSW) current with an amplitude of 18 mA and period of 86 s. The upper panel shows the time variation of the driving BSW current. At t = 1050 s, the BSW drive was switched to + 18 mA dc current for the rest of the relaxation process.

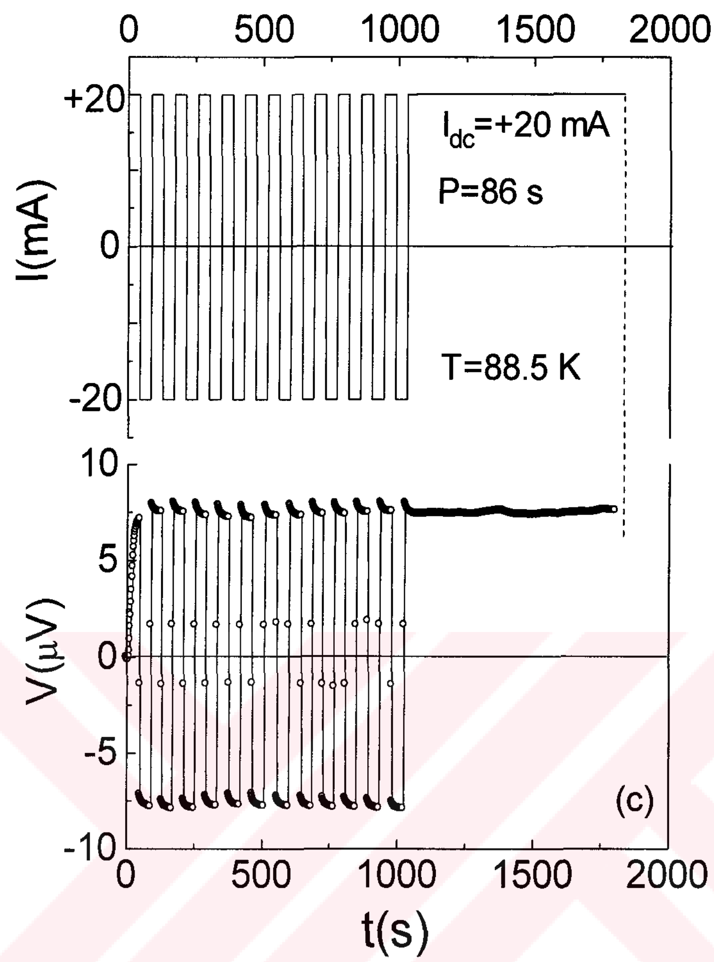

Figure 5.6(c) Long time evolution of the voltage measured at T = 88.5 K for a bi-directional symmetric square wave (BSW) current with an amplitude of 20 mA and a period of 86 s. The upper panel shows the time variation of the driving BSW current. At t = 1050 s, the BSW drive was switched to + 20 mA dc current for the rest of the relaxation process.

5.3.2 Time Evolution of the *V-t* Curves for BSW Currents with Short Period and Different Amplitudes at Different Temperatures: Observation of Voltage Oscillations

Figures 5.7(a) to 5.7(d) shows the time evolution of sample voltage measured at $T = 85.5$ K for BSW current with a period $P = 20$ s and different amplitudes of 9, 11, 12 and 13 mA, respectively. The upper panels in Fig.5.7 represent the time variation of the driving current. The experimental V - t curves consist of two different regimes. One of them is the development of a sharp increase in sample voltage during the first half-cycle of BSW current; the other regime is characterized by nearly periodic sinusoidal-type oscillations of voltage in the rest of the full time scale of the experiment. These regular voltage oscillations in the V - t curves appear after approximately one complete cycle of the driving BSW current (i.e., at around t = 20 s), and the period of the oscillations is almost same as that of the drive. Another observation is the gradual increase in the amplitude of the oscillations as the amplitude of the driving current is increased from 9 to 12 mA. The amplitude of oscillations takes its highest value when the BSW amplitude is 12 mA, and the oscillations become more regular and more pronounced. Interestingly, increasing of the amplitude of driving current from

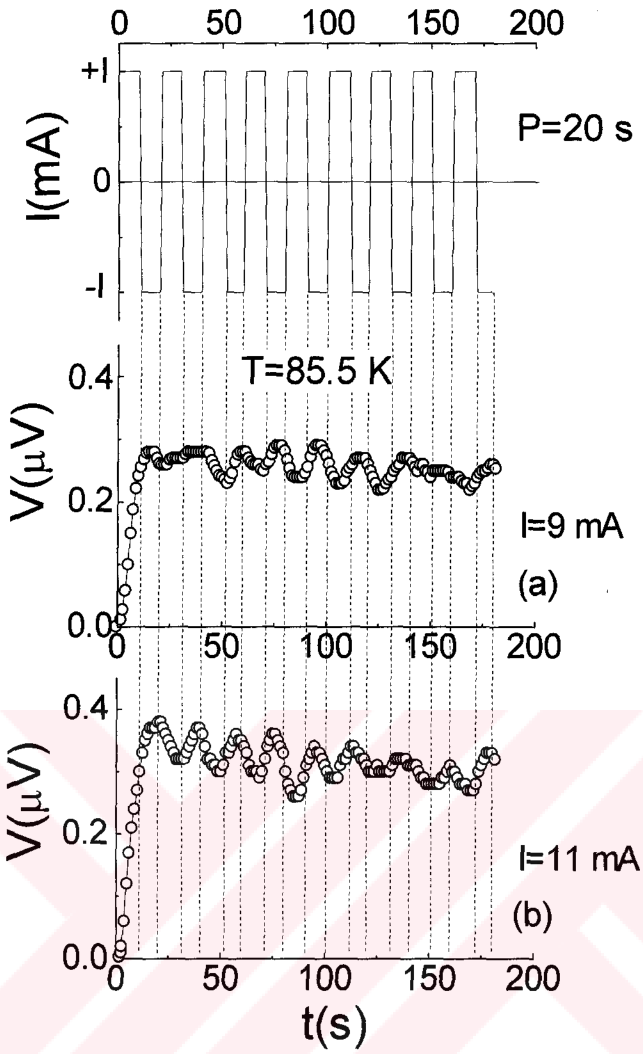

Figure 5.7 Time evolution of sample voltage measured at T = 85.5 K for a BSW current with different amplitudes of **(a)** I = 9 mA, **(b)** I = 11 mA, **(c)** I = 12 mA, and **(d)** I = 13 mA. The top panel represents BSW current with a period P = 20 s.

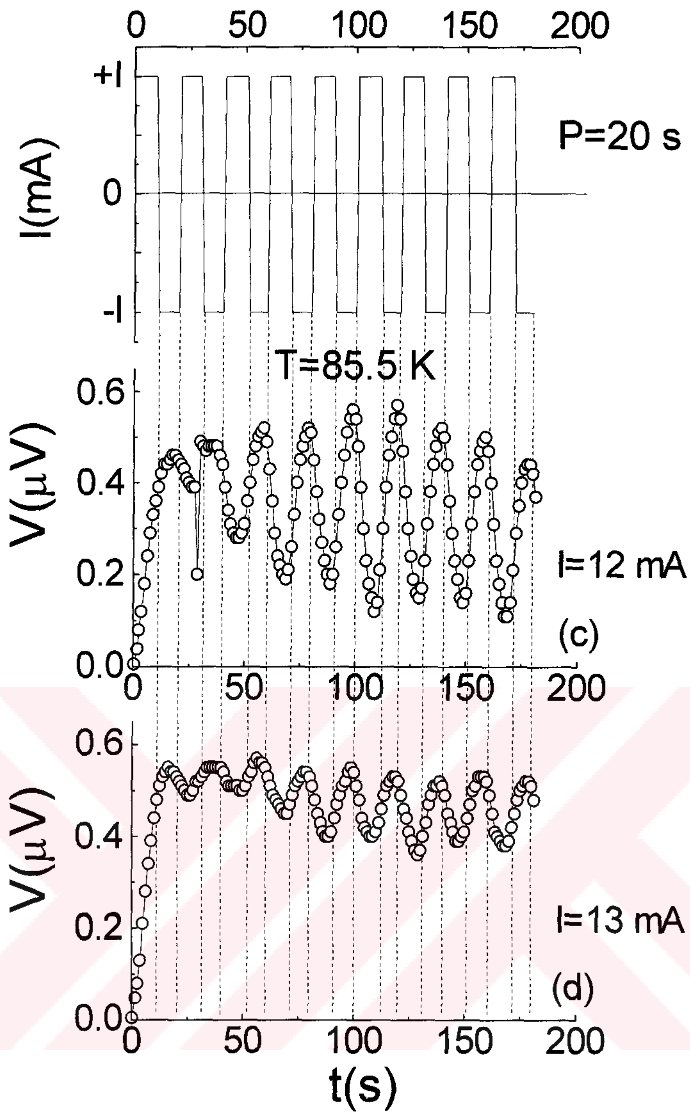

(Continued)

I = 12 mA to 13 mA causes a marked decrease in amplitude of oscillations. This implies that, in a given temperature range, the amplitude of oscillations passes through a maximum for certain values of both the amplitude and period of driving BSW current. On the other hand, although the driving current is bi-directional, the voltage oscillations in Figs. 5.7(a) – 5.7(d) remain always positive. It appears that the moving entity does not exactly follow the change of the polarity of the driving current, and the oscillations develop on a time-independent background which increases slightly with the amplitude of bi-directional current.

5.3.3 Influence of the Period of BSW Current on the Voltage Oscillations

To assess the influence of changes in the period of bi-directional square wave (BSW) current on the voltage oscillations, V - t measurements were carried out at 85.5 K for a BSW current with different periods at a fixed amplitude of 13 mA. Figures 5.8(a) and 5.8(b) show the V - t curves obtained for the periods of P = 40 and 75 s, respectively. The upper panel in each diagram depicts the BSW current. Regular sinusoidal-type voltage oscillations are observed for P = 40 s (Fig. 5.8(a)), which are similar to those in Figs. 5.7(a) – 5.7(c). After the first cycle of BSW current, the oscillations evolve for a while in opposite phase to the driving current, whereas, the phase difference between the voltage oscillations and driving current gradually disappears at sufficiently long times. For the BSW current with a period of 75 s, the voltage oscillations undergo a distortion in time by exhibiting a behavior similar to the functional change of driving current (Fig. 5.8(b)). We note that the voltage oscillations shown in Fig. 5.8(b) evolve in opposite phase to the driving current after the first cycle, contrary to the case in Fig. 5.8(a), and this phase relation is kept within the full time scale of the measurement. In addition, a direct comparison of Fig. 5.7(d) with Figs. 5.8(a) and 5.8(b) shows that the

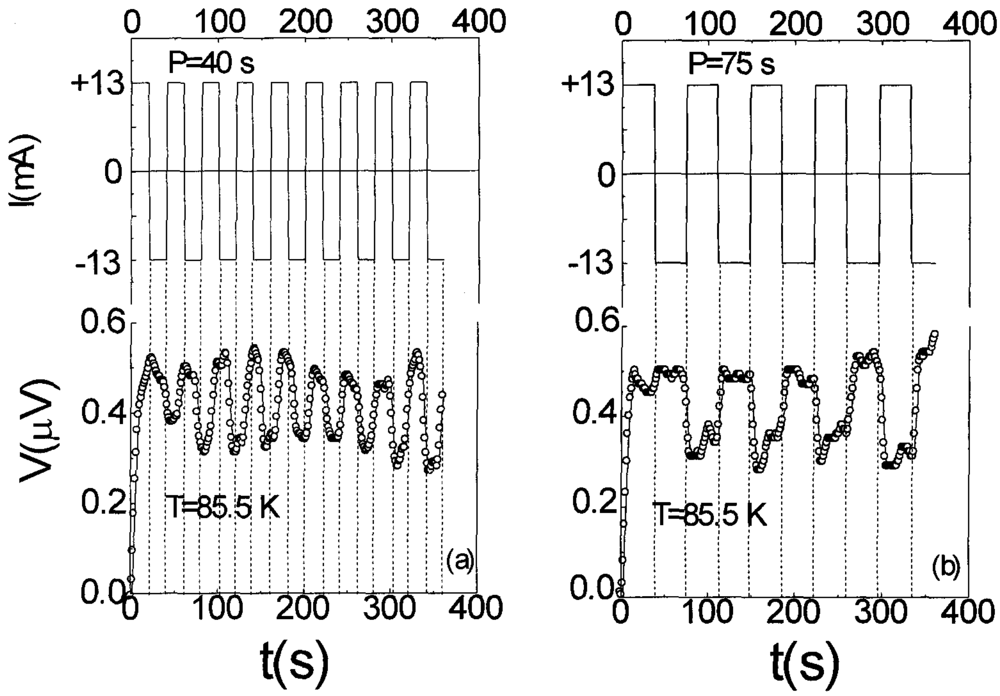

Figure 5.8 Time evolution of the sample voltage measured at 85.5 K for BSW current with amplitude of 13 mA and period. **(a)** $P = 40$ s and **(b)** $P = 75$ s. The upper panels show the time variation of the BSW current.

amplitude of oscillations becomes significantly larger as the period of driving current is increased, although the amplitude of the drive and temperature do not change. For instance, the average amplitude of oscillations in Fig. 5.7(d) is about 0.15 μV for $P = 20$ s, while,that in Fig.5.8(b) for $P = 75$ s, it is about 0.25 μV.

5.3.4 Comparison of Influences of dc and BSW Driving Currents on the *V-t* curve

Figure 5.9 shows the results of measurements carried out at $T = 85$ K for BSW current with an amplitude of 20 mA and a period of 20 s over a time range from 0

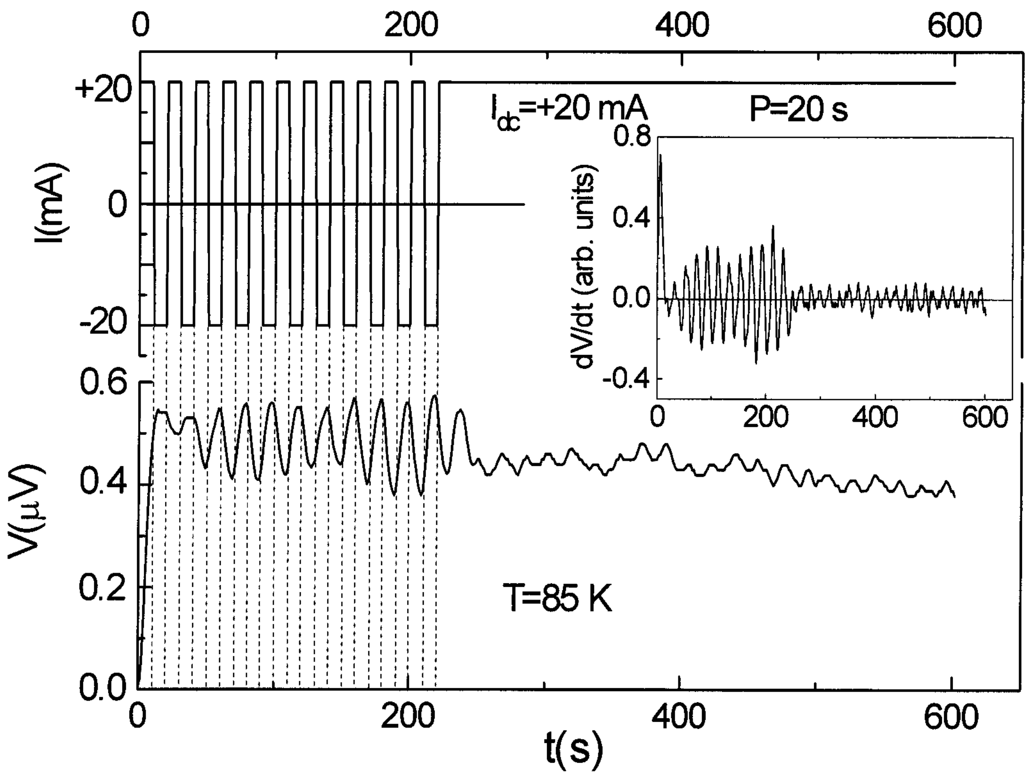

Figure 5.9 Long time evolution of the sample voltage measured at T = 85 K for BSW current with a period of 20 s and amplitude of 20 mA (upper panel). The driving current was switched to + 20 mA dc current at around t = 220 s. The inset shows the time derivative of the sample voltage.

to 220 s. In order to see the influence of the dc current on the time evolution of sample voltage, at around t = 220 s, the BSW current was switched to + 20 mA dc current for the rest of the relaxation process. The period of the regular oscillations in sample voltage are less than that of the BSW current. After switching to dc current, the regular voltage oscillations disappear, and the observed voltage signal is in the appearance of a noise signal. To demonstrate better the sinusoidal-type oscillations and remove the background voltage in the experimental V - t curve, we calculated the first derivative of the V - t curve with respect to time and plotted as an inset in Fig. 5.9. The first derivative shows that the oscillations evolving inside the sample are physical, not artifact.

5.3.5 Influence of Amplitude of BSW Current with Long Period on the *V-t* curves

Figures 5.10(a)-5.10(f) show the V - t curves measured at T = 81.5 K for BSW current with a period of 75 s and amplitude of 40, 43, 45, 46, 47 and 50 mA, respectively. The regular sinusoidal-type oscillations appear after the first half period of the driving current. However, as the amplitude of the applied BSW current is increased, distortion in the oscillations appears, which becomes progressively more pronounced (Figs.5.10(b) - 5.10(f)). This implies that the oscillations are fairly sensitive to the magnitude of the driving current. Furthermore, we note that the sample voltage is in opposite phase to the drive for the current amplitudes of I = 43, 45, 46 and 47 mA. On the other hand, when the current amplitude is 50 mA, the sample voltage begins to follow the drive and the phase difference between them disappears (Fig. 5.10(f)). Note also that the responses in Figs. 5.10(e) and 5.10(f) corresponding to the driving currents of 47 and 50 mA become totally different as compared to that of observed in V - t curves for smaller currents: In these V - t curves, the sample voltage takes positive and negative values so that a symmetric behavior, which reflects the change of polarity of the driving current, is observed. Another common feature of the V - t curves shown in Figs. 5.10(b) and 5.10(f) is that absolute value of the sample voltage tends to decrease or increase within the time intervals where the amplitude

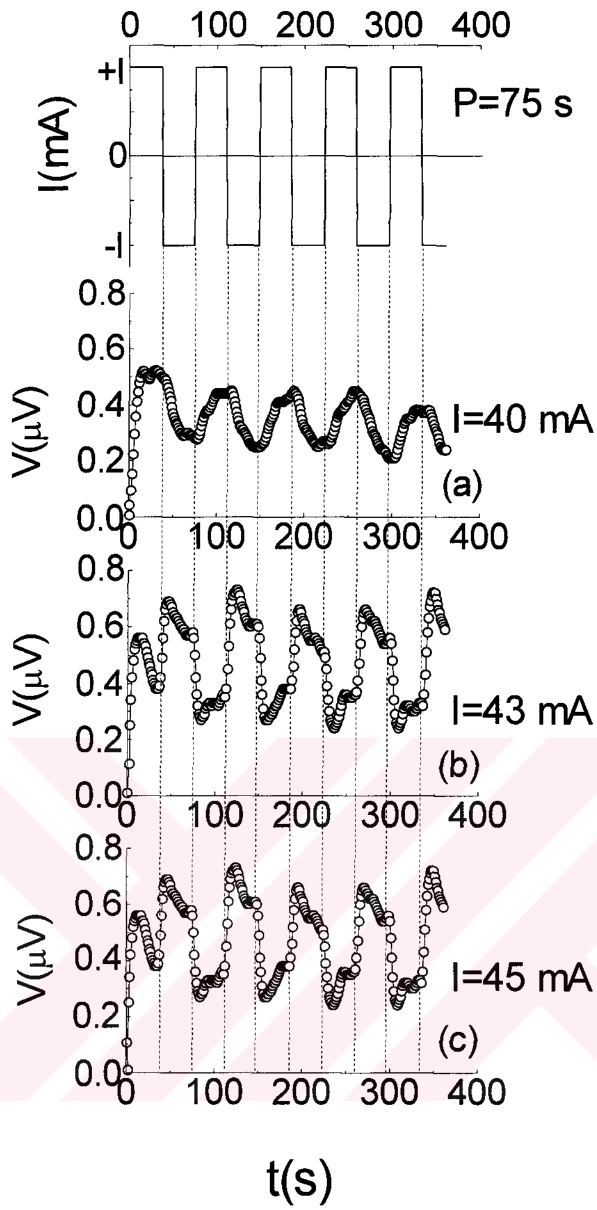

Figure 5.10 Time evolution of the sample voltage measured at T = 81.5 K for BSW current with a period of 75 s and amplitude of **(a)** 40 mA, **(b)** 43 mA, **(c)** 45 mA, **(d)** 46 mA, **(e)** 47 mA, and **(f)** 50 mA. The upper panels show the time variation of the drive.

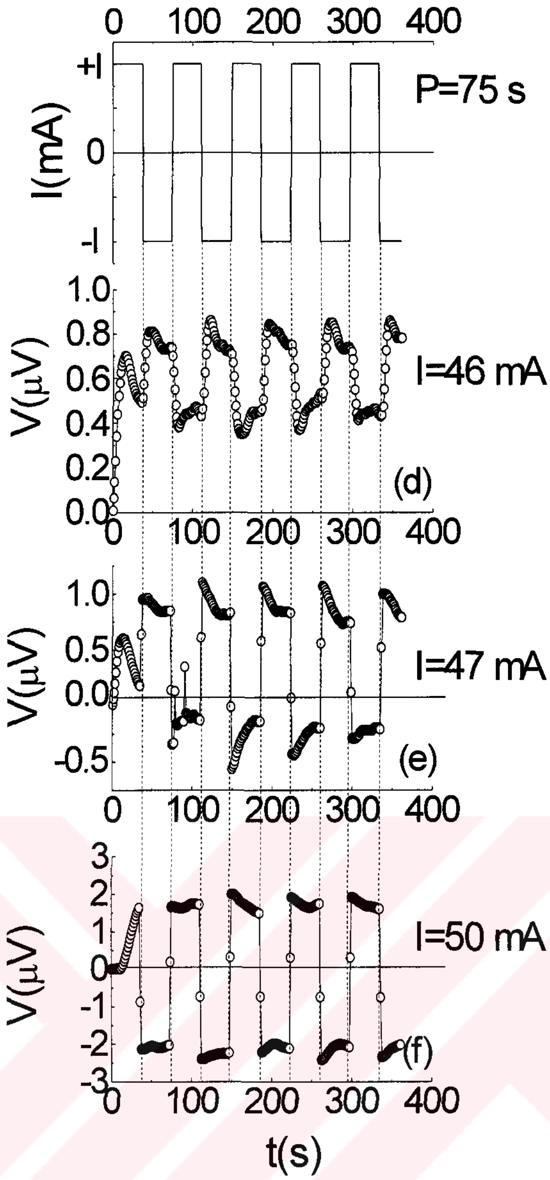

(Continued)

of driving current remains constant. In fact, it can be expected that BSW currents having long periods (75 s) cause relaxation effects in the V - t curves depending on the amplitude of the driving current. This finding indicates that the period of the driving current has a substantial effect on the evolution of V - t curves.

5.3.6 Reobservation of Oscillatory Behavior of Voltage Response: Correlations with Amplitude and Period of Driving Current

Figures 5.11(a)-5.11(c) show the V - t curves measured at T = 81.5 K for a BSW current with amplitude of 45 mA and different periods of P = 10, 20 and 40 s, respectively. The measurements were carried out in a time interval of 0 - 360 s.

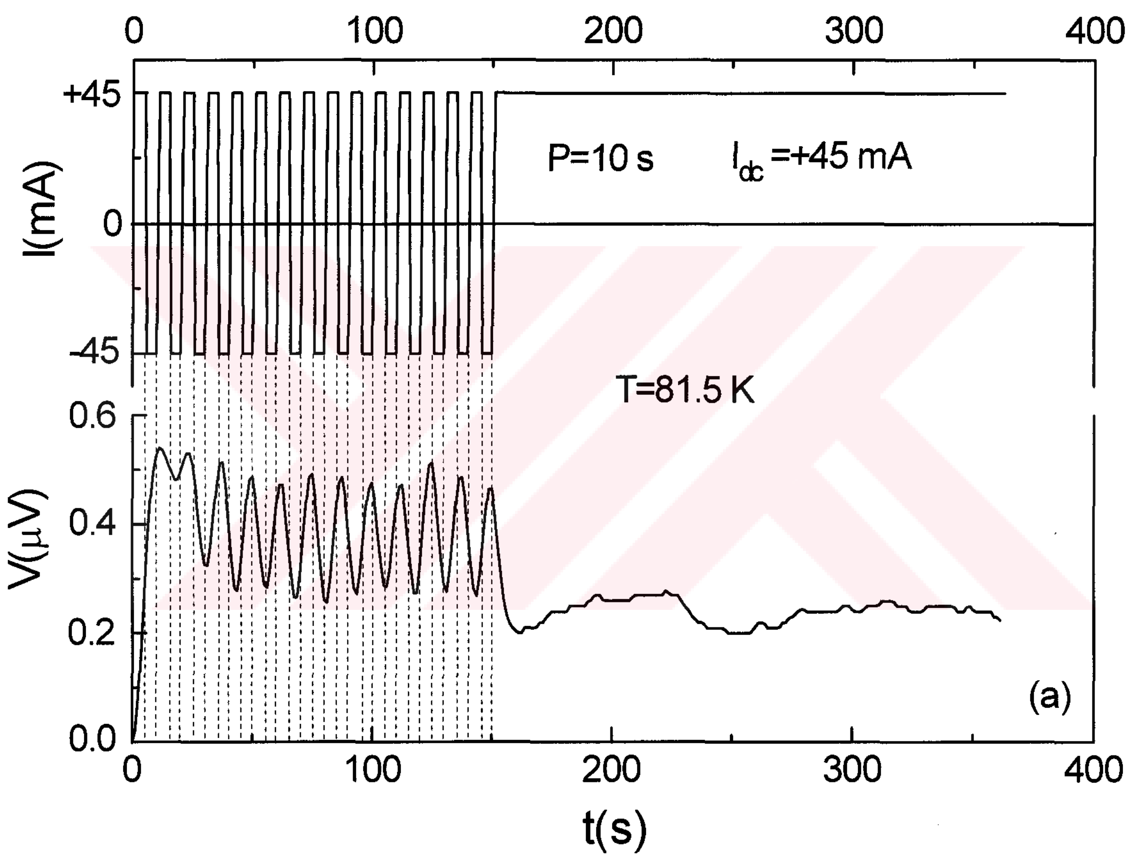

Figure 5.11(a) Voltage oscillations for BSW current with a constant amplitude (45 mA) and a period of 10 s recorded at T = 81.5 K. The drive is switched to dc current of + 45 mA at t = 150 s.

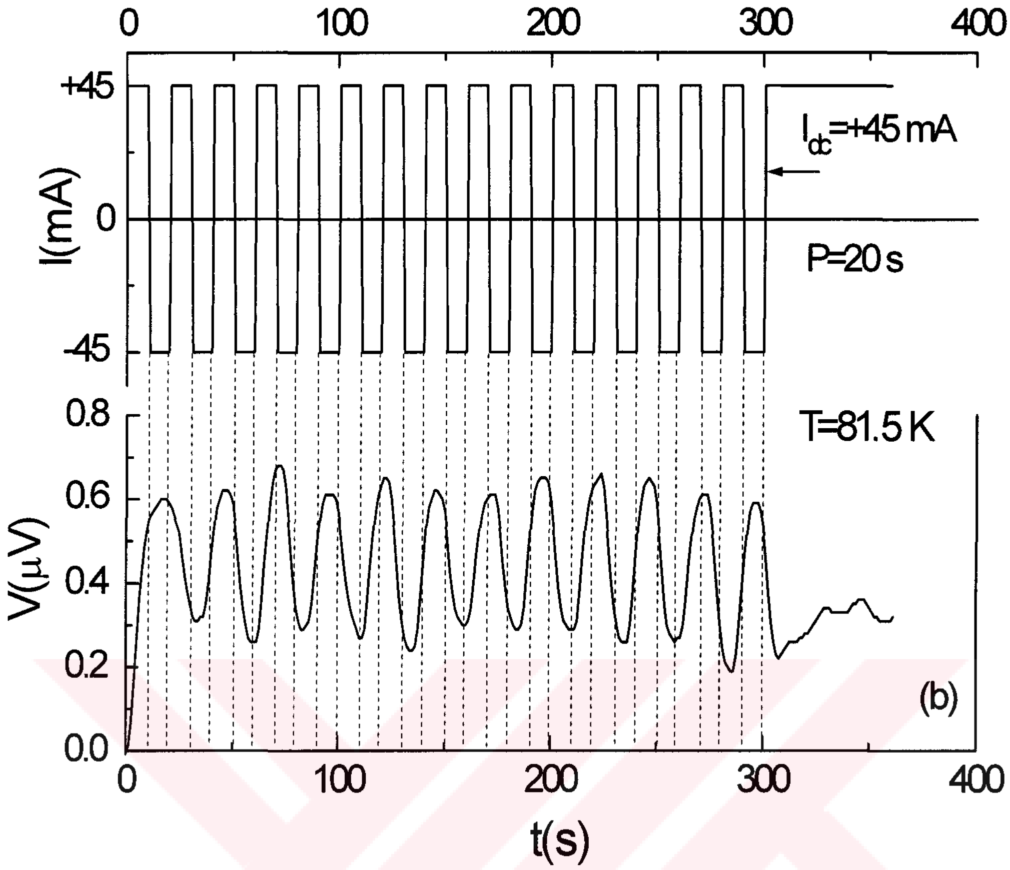

Figure 5.11(b) Voltage oscillations for BSW current with a constant amplitude of (45 mA) and a period of 20 s recorded at T = 81.5 K. The BSW drive is switched to dc current of + 45 mA at t = 300 s.

As can be seen from the V - t curves in Fig.5.11, regular sinusoidal-type oscillations appear as the period of the drive decreases, whereas, pronounced distortions in sample voltage were observed for longer period (75 s) at the same current amplitude (see Fig. 5.10(c)). In addition, it is seen from Fig.5.11(c) that increase in the period of drive (P = 40 s) leads to re-appearance of the distortions in sample voltage. With the aim to compare the effects of BSW current with that of dc current on the evolution of V - t curves, after BSW current was applied

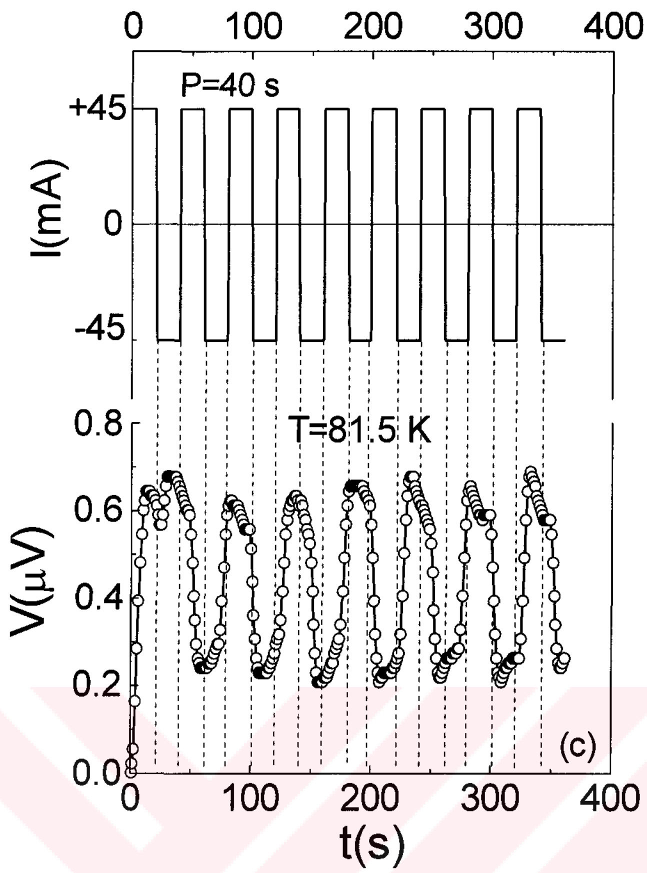

Figure 5.11(c) Voltage oscillations for a BSW current with a constant amplitude (45 mA) and a period of 40 s recorded at T = 81.5 K.

several times, the driving current was switched to dc current of + 45 mA at t = 150 and 300 s. The results are given in Fig. 5.11(a) and in Fig.5.11(b), respectively. The sinusoidal-type oscillations disappear as the BSW current is switched to dc current and then a pattern similar to noise measurements is observed.

CHAPTER 6

DISCUSSION

6.1 Time Effects and the Evolution of V - t curves in Two or Three Stages

We now discuss on the V - t data presented in Figs. 5.2(a), 5.3(a), 5.4, and some of the V - t curves in Fig. 5.5 which evolve in two or three stages over time. We suggest that, in the V - t curves with two stages for a current value of I_1, at the beginning, the transport current tries to distribute itself and meanders along the nonresistive flow channels for a while. As the time proceeds, the internal energy of the superconducting material may increase due to the presence of the transport current so that the effective superconducting order parameter can not keep its previous spatial configuration and thus an increase in sample voltage may be observed. This means that, the transport current penetrates the weak-link network where the weak superconducting regions exists and disrupts them gradually [35]. As a result, an enhancement in dissipation together with a dynamic process triggered by the current will appear. The nonlinear increase in sample voltage observed in this stage can be evaluated as an indication of the coexistence of the disruption and reconstruction of the weak-link structure by the transport current. However, the voltage response shows that the competition between these two physical mechanisms develops mostly in favor of disruption in time. Finally, at second stage, the transport current nearly completes the redistribution process depending on its magnitude and a steady process is established within the time scale of the experiment.

On the other hand, the V - t curves in Figs. 5.5(a), 5.5(i) and 5.5(l) evolve in three stages. Initially, it is seen that there is no measurable voltage to record. A similar process is observed in Figs. 5.2(a) and 5.3(a) as well, however, it evolves in shorter times. As is noted, the time required for this process increases as the magnitude of current I_1 is decreased. We suggest that the delay appearing in the V - t curves can be attributed to the fact that the effective superconducting order parameter maintains its prior spatial configuration, depending on the magnitude of the driving current, while the driving current tries to organize itself inside the sample. Thus, when the order parameter is suppressed by the transport current, a measurable voltage develops across the sample.

6.2 Quenched State for Currents $I_1 > I_2$ at Different Temperatures

We consider the time effects induced by the dc transport current in shown Figs. 5.2(a), 5.3(a), and 5.4, and discuss the influences of different transport currents and the temperature on evolution of the V - t curves. When the transport current is interrupted, it was observed that the sample voltage becomes zero immediately after the current is turned off. It can be suggested that the weak links form a coherent state and the resistive flow channels disappear within a very short time. Thus, the effective order parameter should increase after the interruption of transport current. These experiments can be considered as a test of whether the thermal relaxation due to the Joule heating at current contacts exists or not. Our data demonstrate that the observation of zero voltage for $I = 0$ (just after the dc current was turned off) rules out the thermal relaxation associated with Joule heating effects.

The decrease of transport current from I_1 to a smaller value of I_2 causes the appearance of a different voltage response. Following this procedure, the effective superconducting order parameter suppressed by I_1 is enhanced rapidly, and a quenched state associated with the distribution of the transport current is developed. Depending on the magnitude of the currents I_1 and I_2, and the temperature range of measurements, the quenched state reorganizes itself over time and evolves to low dissipation levels. The decay in sample voltage can be considered as a measure of this reorganization process in which the structural disorder, chemical and anisotropic states of the sample play a central role. At relatively low currents, the order parameter enhances in time and the effective size of dissipative non-superconducting flow channels begins to decrease gradually with time and, thus, the superconducting state could be reached. At low enough currents, these channels are closed completely within a very short time, so that the response is voltage decay with transition to superconducting state.

We also correlate the voltage decays without transition and the smooth transitions appearing in V - t curves to the glassy state relaxation (GSR), as in the case of spin glasses [29, 32]. It should be noted that the physical case appearing in V - t curve can not be explained alone by the usual phenomenological theories such as flux creep theory [24], collective creep model [28] etc., since these theories do not explain sufficiently the transition process evolving from resistive state to true superconducting state. It has already been shown [29, 33] that such type of relaxation can be explained by considering the hierarchy of energy barriers together with the existence of large number of energy states. Within this description, it is assumed that the energy difference between the neighboring barriers is small, while the difference between the more distant barriers is much higher (see Fig. 3.1). Due to the thermal activation, the vortices can overcome easily the neighboring barriers, but fall in a deeper barrier (see Fig. 3.1). Such an energy landscape directly leads to the concept of the superconducting glass model [29]. This model also gives useful results about the decay of voltage of both zero (magnetic) field cooled and field cooled sample below T_c [29, 33].

As is outlined in Chapter 3, one of the requirements of GSR is that the voltage must decrease exponentially in time as in Eq. 3.2. The solid lines through experimental data points in Figs. 5.2(a), 5.3(a) and 5.4 are calculated by using Eq. 3.2. The reasonable agreement between the calculated curves and the experimental data suggests that the quenched state is closely related to GSR relaxation. The characteristic time τ_0 values found from the fitting of Eq. 3.2 to the experimental V - t curves given in Figs. 5.2(a), 5.3(a) and 5.4 are plotted as a function of the driving current (I_2) in Fig. 6.1. The characteristic time τ_o tends to increase with current, because the transitions at low currents are more faster than that at higher currents. In addition, we note that there is no marked change in values of τ_o as the temperature or the current I_1 is reduced (Fig. 6.1). One of the

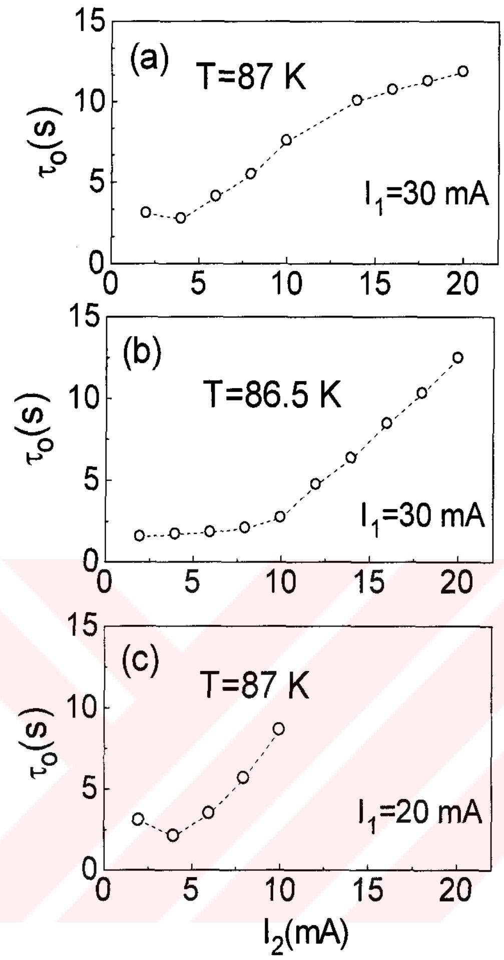

Figure 6.1 Variation of the characteristic time τ_o with current I_2 : **(a)** Extracted from Fig. 5.2(a) **(b)** Extracted from Fig. 5.3(a) and its inset **(c)** Extracted from Fig. 5.4. The dashed lines are a guide for eye.

important points what we wish to emphasize here is that the time evolution of the V - t curves given in Figs. 5.2(a), 5.3(a), and 5.4 also depict the time dependence of the order parameter, that is, the relaxation of the order parameter over time. As noted previously in section 2.5.2, according to the Ginzburg-Landau (GL) theory and time-dependent GL theory, the superconducting order parameter depends explicitly on time, temperature, current density, and external magnetic field [3, 18, 21]. We suggest that the experimental procedure used in the acquisition of V - t curves presented in Figs. 5.2(a), 5.3(a) and 5.4 provides a useful way to monitor the time variation of order parameter, in details. All these facts underline the importance of the V - t curve and show that, in addition to the usual transport measurements, this experimental method is a candidate to be one of the powerful tools to characterize the superconducting materials.

It is also observed that the decrease in the initial transport current I_1 (see Figs. 5.2(a) and 5.4) or the increase in sample temperature (see Figs. 5.2(a) and 5.3(a)) do the same physical impact. The transport current serves here as an "effective temperature" in the sense defined in the statistical mechanics, and anneals dynamically the corresponding states during the relaxation process [5, 36, 37]. Further, the magnitude of the transport current determines mainly the annealing kinetics. Therefore, it can be suggested that there must be a correlation between the high transport currents and the high temperatures. In fact, this is a natural consequence of the order parameter, which depends strongly on both the temperature and transport current.

6.3 Residual Voltage V_r and Its Appearance and Relaxation

Another interesting feature of the experiments carried out in this study is the appearance of a residual voltage (V_r) in V - t curves illustrated in Fig. 5.5 [except those given Figs. 5.5(a), 5.5(g), 5.5(i) and 5.5(l)]. In order to observe the residual voltage, the condition $I_1 < I_2$ must be satisfied in the previous measurement. In the next experiment, a residual voltage appears in $V - t$ curves, irrespective of the conditions $I_1 > I_2$ or $I_1 < I_2$. In the case of $I_2 < I_1$, we suggest that the nonsuperconducting resistive flow channels formed by the transport current do not find enough time to decrease their size, due to the strong suppression of the order parameter, and it seems that a kind of short lived metastable state evolves through the sample.

Here, the role of the transport current is twofold: one is to reduce the effective pinning potential and to release the residual voltage trapped in the sample, the other is to help to allow the metastable state to live long. Indeed, at low currents the life time of the metastable state is shorter than that at higher currents; this can be seen from the time passed to reach the superconducting state as observed in the V - t curves illustrated in Figs. 5.5(e), 5.5(j) and 5.5(m). In this picture, the quenched state (or the associated order parameter) reorganizes itself with the help of the transport current through the sample and explores energetically low new states as the time proceeds. Under the condition $I_1 > I_2$, the newly formed nonsuperconducting flow channels developed inside the sample are added to the ones formed previously and to the ones who did not find enough time to be closed in the previous experiment. Therefore, the dissipation continues to increase in time.

In order to remove the residual voltage trapped in the sample, and, thus, to form a coherent state, the initial current I_1 must be interrupted or reduced to sufficiently lower values so that the superconducting state occurs, that is, the sample voltage to become zero. As a consequence the residual voltage is removed completely [Figs. 5.5(g), 5.5(j) and 5.5(l)]. A comparison between Fig. 5.5(i) and Fig. 5.5(j) shows that the time passed between two successive experiments influences the experimental V - t curves. To eliminate the effect of the residual voltage, one should leave enough time between two successive experiments, or an extra experiment should be performed in the mean time, in which the initial current I_1 is reduced to a sufficiently low value I_2 to satisfy zero sample voltage.

6.4 Current-Induced Organization of Vortices and Voltage Oscillations

It has been shown that the dynamics of the vortices in Type-II superconductors depends also on the type of the transport current modulations [7, 38, 39]. The experimental studies established that the direct current, alternating current, square wave and asymmetric square wave currents cause several effects [7, 38, 39]. For instance, high vortex mobility appears for alternating currents, but no apparent vortex motion for direct currents [7, 39]. Henderson *et al.* [7] have investigated the vortex dynamics in a single crystal sample of 2H-$NbSe_2$ by observing how the current driven ordering of moving state evolves when the driving current is changed. Such fast transport measurements performed by Henderson *et al.* [7] showed that the response includes three distinct regimes depending on the type of current: No measurable voltage for a dc driving current, a voltage growing from zero for a bi-directional square wave (BSW) current, and a decay in voltage for a dc current. Our experiments for a square wave current show clearly the current driven re-ordering of vortices since the response grows with every current reversal.

In the noise measurements carried out on a detwinned YBCO single crystal below the melting transition by D'anna *et al.* [40], the origin of the voltage oscillations was attributed to the surface barrier which influences the coherent motion of the vortices entering or leaving through the large faces of the crystal. Gordeev *et al.* [38, 39] showed that an asymmetric square wave current causes low-frequency periodic voltage oscillations in detwinned single crystal YBCO sample below the vortex lattice melting temperature in the presence of an external magnetic field of 2 T. They reported that the temporal asymmetry in square wave current and its periodic reversal are essential to observe such regular oscillations. Further, they attributed the regular oscillations to the transit of periodic vortex density fluctuations which is similar to the dynamics of the charge density waves (CDWs) driven by a sufficiently large driving force [41 - 55]. A similar study was carried out by Kwok *et al.* [56]. They attributed the observation of the oscillatory instability in single crystal YBCO sample to the strong competition between the driving and pinning forces and correlated it to the elasticity of the vortex solid and the long time relaxation effects.

In chapter 5, some of the experimental results associated with the type of the transport current used in present measurements have a direct effect on the evolution of the V - t curves provided that some requirements are satisfied. We first discuss the influence of a BSW current on the evolution of the V - t curves. First of all, we would like to note some similarities between the present study and that by Gordeev *et al.* although they used a single crystal sample of YBCO: The voltage oscillations are observed for BSW current and the amplitude of the response is of the same order, i.e., in the range from 10^{-7} to 10^{-6} V. In addition, in the study by Kwok *et al.*, [56] nearly the same range is found for a periodic sinusoidal drive. In this work, for the first time, we observed similar long periodic oscillations of response for a drive in the form of BSW current in a polycrystalline YBCO sample.

However, before going into the details of discussion, to better describe the V - t curves presented in Figs. 5.1 to 5.11, we should point out that the voltage developing across the sample arises from the motion of the self-magnetic flux (SMF) lines induced by the transport current. The self-magnetic field B_s induced by the applied transport current can be calculated by using the Maxwell equations [57-59]. For a sample in the shape of the rectangular prism, B_s becomes equal to

$$B_s = \mu_o \gamma J = \mu_o J \cdot \frac{wt}{2(w+d)}, \tag{6.1}$$

Where J is the current density, μ_o is the permeability of free space ($\mu_o = 4\pi x 10^{-7}$ H/m), γ is the geometric parameter of the sample and given as $\gamma = wt/2(w+d)$, w

is the width, and d is the thickness of the sample. The slap used for the transport measurements has dimension of length l ~ 4 mm, width w ~ 0.1 mm, and thickness d ~ 0.2 mm. Thus, the self-field is found as ~ 0.2 mT for a transport current of 50 mA. It may be that the transport current values used in our measurements (or the self-magnetic field induced by the transport current) are sufficiently weak to suppress the superconducting order parameter. However, the order of the voltage (~ 10^{-7} – 10^{-6} V) recorded in the present measurements bears this idea out. We note that the flux lines associated with the self-field of the transport current are concentrated in the intergranular region. This description shows that the time effects in V - t curves originates essentially from the intergranular region where the dynamics of the Josephson vortices develops [5, 35, 37].

The sharp increase in sample voltage at the beginning of the measurement observed in the oscillating V - t curves can be interpreted in the frame of physical case described for ones with two or three stages. Therefore, we do not intend to discuss it in details. In the final stage, the response manifests itself as voltage oscillations evolving in sinusoidal-like or non-sinusoidal types, which follow generally the lineshape and period of the driving current. The presence of regular sinusoidal-like voltage oscillations [see Figs. 5.7, 5.8(a), 5.9, 5.10(a), 5.11 and 5.12] depends strongly on the amplitude and period of the BSW current.

The coherent oscillations in the V - t curves suggest that the majority of SMF lines, which are in motion, drifts across the sample and remains in an oscillating mode that is easily resolved in our experiments. At this point, it is necessary to recall the role and importance of pinning on the evolution of V - t curves, since the type of pinning centers and the pinning strength determine the flow pattern of flux lines evolving inside the sample. We suggest that the regular sinusoidal type oscillations arise from a strong dynamic competition between pinning and depinning processes [56]. This is one of the main reasons why the regularities or distortions appeared in the evolution of some of the V - t curves show a strong dependence on the period and magnitude of the driving current. Indeed, at long periods or/and large amplitude of the drive, this competition reflects itself as significant relaxation effects, which correspond to a decrease or increase in sample voltage [see, for instance, Figs. 5.6(a)-5.6(c), 5.8(b) and 5.10(b) – 5.10(f)]. This indicates that the moving entity explores new accessible states and tries to go to a new equilibrium state in time. We note that Henderson *et al.* [6] and Xiao *et al.* [33] have also observed such time effects in fast transport measurements in a single crystal sample of 2H-$NbSe_2$ and interpreted the decay in voltage in terms of a glassy state relaxation (GSR) characterized by an expression of $V(t) \sim \exp(-t/\tau_0)$, where τ_0 is a characteristic time. We should note that an attempt to fit our data corresponding to the voltage decays appeared at long period of drives (see, Figs. 5.10(b) to 5.10(e)) to this expression gives unsatisfactory results. In addition, the regular sinusoidal-type oscillations also indicate that the interaction between SMF lines and pinning centers could be semi-elastic rather than elastic coupling. In this description, the oscillating mode could be closely related to the defective flow of SMF lines in which some of them are moving and the others remain pinned, i.e., non-uniform flux motion [7, 35, 38, 39]. Such a flow pattern is a prominent feature of plastic regime [60 - 64]. Many recent realistic computer simulations revealed that, at low currents (or at low driving force), the vortex lattice becomes highly defective and exhibits several different plastic flow regimes due to the pinning strength. For instance, in a recent study, Olson *et al.* [62] showed the presence of semi-elastic flow regime due to the pinning strength by using large-scale molecular dynamic simulations. Their study gave a measurable voltage noise spectrum which could be changed by adjusting the degree of the dynamic competition between pinning and de-pinning. We believe that appearance or disappearance of the phase difference between the response and the BSW drive originates from this dynamic competition and also from the strong diamagnetic response of the sample to the drive in a complicated way. At low dissipation levels, the moving entity does not respond immediately to the drive, since pinning is effective and dominates the motion of SMF lines, and, thus, a delay which causes a phase difference between the response and drive appears.

We note that, in our measurements, the response generally oscillates with the period of BSW drive. The fast Fourier transform (FFT) of the corresponding V - t curve can be taken to determine the spectral content of the oscillations. A typical example concerning the FFT of the V - t data given in Figs. 5.11(a) to 5.11(c) is illustrated in Figs. 6.2(a) to 6.2(c), respectively. The FFTs show that there is a fundamental frequency accompanied by its harmonics. The fundamental periods ($P_{\text{Vosc,FFT}}$) found from the FFT of oscillations in Figs. 5.11(a) to 5.11(c) are 11.7 s, 23.4 s and 46.5 s, respectively. Note that the values of $P_{\text{Vosc,FFT}}$ are comparable to actual periods of the corresponding BSW drive, i.e., P = 10, 20 and 40 s. This finding suggests the presence of a dynamic physical case, which resembles the driven charge density waves (CDWs) by an external drive. It has been already argued by Gordeev *et al.* [38] that the system of weakly pinned vortices is similar to the pinned CDW state. Experimental studies on CDW revealed that, in a current or voltage controlled experiment, coherent voltage or coherent current

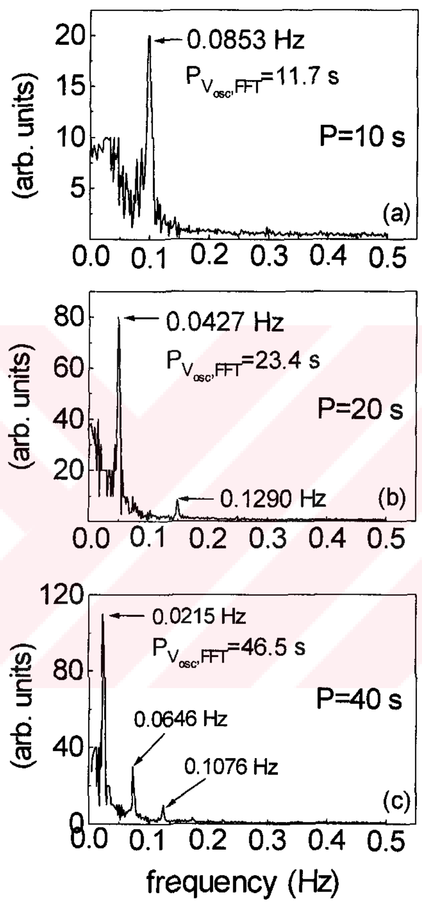

Figure 6.2 Fast Fourier Transform of the V - t curves given in Fig. 5.11(a) to 5.11(c) measured at 81.5 K for BSW drive with amplitude 45 mA and period 10 s, 20 s and 40 s, respectively. The fundamental frequencies and their harmonics are marked on the curves. The fundamental period $P_{\mathrm{Vosc,\ FFT}}$ found from FFTs is also given along with the periods of BSW current.

oscillations appear across the sample after a threshold value of the driving current [43, 45, 52, 55]. In addition, it has been shown that the sliding CDW can cause coherent oscillations at well defined frequencies of the drive [46 - 48]. It is well known that CDW's are characterized by an order parameter which has an amplitude and a phase [44, 49]. A phenomenological theory, which considers an order parameter correlated to the superconducting state, was proposed by Ginsburg and Landau (GL) a few decades ago. Both the GL theory and its extended versions, such as time-dependent GL theory, predict the spatial variation of the order parameter which is in reasonable agreement with the physical expectations.

Above we noted the similarities between the physical case in our measurements and the driven CDW's. On the basis of these similarities, as a first approximation, we suggest that a physical mechanism concerning the density fluctuations associated with SMF lines can be introduced. Such coherent density fluctuations in the sample can develop and can do a similar effect along with the dynamic competition between pinning and de-pinning as in the case of the CDW's. Nevertheless, we feel that this point needs further experimental and theoretical investigations.

We now discuss the role of the polarity change of the driving current on the evolution of the V - t curves. Note that change in the polarity of the driving current is essential for establishing the regular voltage oscillations, as in the study of Gordeev *et al.* [38, 39]. This requirement is underlined clearly in the V - t curves given in the inset of Fig. 5.9 and also in Figs. 5.11(a) and 5.11(b), where the BSW current is switched to dc current. After switching from BSW to dc current, the voltage oscillations disappear and, the background of the sample voltage decreases somewhat. This finding evidence for another physical effect of BSW current on the evolution of V - t curves: The symmetric forwards and backwards oscillations of the driving current lead to increase in the measured voltage by facilitating the formation and growth of easy motion flow channels for SMF lines inside the sample. The SMF lines in this state are locally ordered and weakly pinned along such easy motion channels which evolve gradually [7]. A similar observation was also reported by Gordeev *et al.* [38]. These authors showed that non-symmetric square wave currents results in higher voltage amplitudes with reduced low noise levels in detwinned YBCO crystals below the vortex-lattice melting temperature, while, a dc current induces highly non-uniform vortex motion. We also note that Henderson *et al.* [7] observed in a single crystal sample of 2H-$NbSe_2$ that the rapid symmetric bi-directional square current pulses cause to a substantial growth in the measured voltage, although they considered a different regime. After several bi-directional pulses, they observed that switching back to dc current results in a considerable decay in the response.

Our experiments reveal that, in order to obtain regular voltage oscillations, the applied driving current should not exceed the effective Josephson critical current which depends strongly on the features of the random weak-link network and also on the temperature and external magnetic field [5]. The importance of this requirement is established well in Fig. 5.9. A comparison between the V - t curves in Fig. 5.10(a) and Fig. 5.10(b) reveals that a slight increase in the amplitude of the driving current causes a considerable departure from the regular sinusoidal-type voltage oscillations by destroying the semi-elastic coupling between SMF lines and pinning centers. A further increase in the amplitude of driving current causes a response reflecting significantly the change in the polarity of driving current. These observations stress the fact that the magnitude of driving current with respect to effective Josephson critical current has a crucial role in obtaining regular sinusoidal-type voltage oscillations.

Let us consider a single reversible Josephson junction. If a constant current which is greater than the critical current of the junction I_{cj} is applied, a current I_n of normal charge carriers (electrons or holes) must start flowing through the junction. In this case, in addition to the supercurrent I_s, a current I_n associated with the normal charge carriers must take place in the transport phenomena, that is, the total current I must be written as $I = I_s + I_n$ [3]. In fact, the analytical expressions derived for an ideal Josephson junction show that the supercurrent I_s can not exceed the critical current I_{cj} according to the equation $I_s = I_{cj}\sin(\varphi)$, where φ is the phase difference between the superconducting wave functions across the junction. This invokes a well-known model so-called Resistively Shunted Model of the Josephson junction (RSJ) [3]. A schematic circuit diagram which depicts RSJ model is given in Fig. 6.3. The circuit in Fig. 6.3 shows a Josephson junction and a normal resistance (R) connected in parallel to it. However, it should be noted that, practically, it is not easy to satisfy ideal and reversible junctions in a granular polycrystalline sample. Therefore, the effective values of the junction parameters

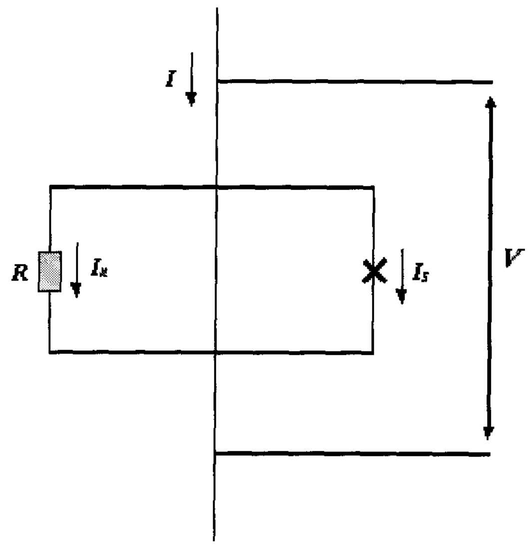

Figure 6.3 Resistively shunted model of the Josephson junction. V is the voltage across the weak link, R is the normal state resistance of the junction and X is the Josephson junction [3].

must be considered in calculations or in the interpretation of the data. We suggest that the V - t curves presented in Fig. 5.10 can be explained in the frame work of RSJ model. As the amplitude of the driving current exceeds the effective Josephson critical current of the medium, a measurable voltage in the direction of the transport current appears so that the sample voltage follows the drive without a phase difference between them. Furthermore, the data in Fig. 5.10 show clearly how to monitor the steps of physical situation associated with RSJ model evolve in time.

On the other hand, the current-induced distortions in oscillations can be avoided by adjusting the period of driving current. For instance, in the V - t curve measured for BSW current with amplitude of 45 mA and period P = 75 s [Fig. 5.10(c)], it is seen that the regular sinusoidal-type oscillations disappear, whereas, for P = 10, 20 and 40 s, they re-appear at the same amplitude and temperature value [Figs. 5.11(a) – 5.11(c)]. This shows that the regular sinusoidal-type oscillations depend not only on the amplitude of driving current, but also on the period of the drive. All experimental observations presented above show clearly the presence of current-induced re-organization of the SMF lines, and underline a fact associated with a new kind of flux dynamics.

Finally, we discuss the type of the vortices which take place in current-induced voltage oscillations. As is well-known, the intergranular currents can be determined by means of transport measurements (resistivity technique), because the intergranular current densities are rather low, and, therefore, easy to measure directly without excessive Joule heating [5, 35, 37, 64, 65]. The intergranular currents can also be measured by the low-field magnetization measurements [5, 64, 65]. For HTSCs, it is commonly accepted that the Josephson vortices can be naturally generated in the weak-link structure of the granular material, and, even in single crystals, the vortices lying between Cu-O layers are in Josephson character [4, 5, 64 - 66]. In addition, it is well known that, inside the superconducting grains, the vortices evolve in the form of Abrikosov-type. We suggest that the voltage oscillations and also the time effects observed in V - t curves measured in this study originate effectively from the intergranular region and, thus, should reflect naturally the oscillations of the flux lines which are of Josephson-type. Recent studies on transport relaxation measurements give a further support for this suggestion [5, 35, 37].

CHAPTER 7

CONCLUSION

In this work, dynamic changes generated by the driving current were studied in superconducting YBCO bulk polycrystalline sample via transport relaxation measurements ($V - t$ curves). The evolution of nonlinear V - t curves was interpreted in terms of the formation of resistive and non-resistive flow channels and the spatial re-organization of the transport current in a multiply connected network of weak-link structure. The dynamic re-organization of driving current could cause an enhancement or suppression in the superconducting order parameter due the magnitude of the driving current and coupling strength of weak-link structure along with the chemical and anisotropic states of the sample as the time proceeds. In addition, when the driving current was interrupted, it was observed that the measured voltage becomes zero. This finding indicated that there is no residual voltage in the sample to be relaxed. However, a nonzero voltage decaying with time, correlated to the quenched state, was recorded when the magnitude of driving current I_1 is reduced to a finite value I_2. It was found that, after sufficiently long waiting time, the evolution of the quenched state could result in a superconducting state, depending on the magnitude of the driving current. We showed that the decays in voltage over time are consistent with an exponential time dependence, ~ $\exp(-t/\tau_o)$, related to the glassy state.

In addition, the influence of bi-directional square wave (BSW) current and dc current on the evolution of the V - t curves were investigated. It was found that a non-linear response in V - t curves to low-frequency BSW driving current reflects itself as regular sinusoidal-type voltage oscillations, while, when BSW current was switched to dc current, the oscillations disappear immediately. The regular sinusoidal-type voltage oscillations were interpreted mainly in terms of the defective flow of current-induced self-magnetic flux (SMF) lines in a multiply connected network, and semi-elastic coupling between SMF lines and pinning centers. The oscillatory behavior of the SMF lines was also discussed on the basis of the similarity between the flux dynamics and charge density waves. Furthermore, it was shown that the voltage oscillations depend strongly on the amplitude and period of BSW current on both short- and long-time scales. Such type of coherent oscillations could also be observed for other temperature ranges, provided that the period and amplitude of the driving current are well adjusted In addition, we found that a change in the polarity of driving current is essential in observing of such oscillations. Furthermore, it was shown that the regular sinusoidal-type voltage oscillations represent a new kind of flux dynamics induced by the transport current.

Finally, it was shown that the experimental methods introduced in this study provide a useful tool to monitor the details of the dynamic changes evolving inside the sample and also measures preciously the time evolution of the superconducting order parameter.

REFERENCES

[1] J. G. Bednorz and K. A. Müller, Z. Phys. B **64**, 189 (1986).

[2] W. Chu, P.H. Hor, R.L. Meng, L. Gao and Z.J. Huang, Science **235**,567, (1987).

[3] V. V. Schmidt, Physics of Superconductors, Introduction to Fundamentals and Applications, Springer-Verlag Berlin, (1997)

[4] E. H. Brandt, Rep. Prog. Phys. **58**, 1475 (1995).

[5] K. Kiliç, A. Kiliç, H. Yetiş, and O. Çetin, Phys. Rev. B, **63**, 144513 (2003).

[6] W. Henderson, E. Y. Andrei , M. J. Higgins, and S. Bhattacharya, Phys. Rev. Lett. 77, 2077 (1996).

[7] W. Henderson, E. Y. Andrei, and M. J. Higgins, Phys. Rev. Lett. **81**, 2532 (1998).

[8] S. N. Gordeev, P. A. J. de Groot, M. Oussena, A. V. Volkozup, S. Pinfold, R. Langan, R. Gagnon, and L. Taillefer Nature **385,** 324 (1997).

[9] C. Kittel, Introduction to Solid State Physics, John Wiley and Sons, 7th Edition, (1996).

[10] A. O. E Animalu, Intermediate Quatum Theory of Crystalline Solids, Princeton-Hall, INC., Englewood Cliffs, New Jersey, (1977).

[11] Z.Z. Sheng, W. Kiehl, J. Bennet, A. El Ali, D. Marsh, G. D. Mooney, F. Arammash, J. Smith, D. Viar, and A.M. Hermann, Appl. Phys. Lett., **52**, 1738 (1988).

[12] A. Shilling, M. Cantoni, J. G. Guo, and H.R. Ott, Nature **332**, 138 (1988).

[13] A. Shilling, M. Cantoni, J. G. Guo and H.R. Ott, Nature **332**, 138, (1988).

[14] C. P. Poole, Jr., Handbook of Superconductivity, Academic Press, (2000).

[15] M. Cyrot and D. Pavuna, Introduction to Superconductivity and High T_c Materials, World Scientific Publishing- Singapure, (1992).

[16] J. Nagamatsu, N. Nakagawa, T. Muranaka, Y. Zenitani and J. Akimitsu, Nature (London), **410**,63 (2001).

[17] C. Buzea and T. Yamashita, Supercon. Sci. Technol., **14**, R115 (2001).

[18] M. Thinkham, Introduction to Superconductivity, 2nd Edition, Mc Graw-Hill Inc, P. 319 (1996).

[19] V. L. Ginzburg and L. D. Landau, Zh. Eksperim. Theor. Fiz. **20**, 1064 (1950).

[20] A. A. Abrikosov, JETP, **5**, 1174 (1957).

[21] A. A. Abrikosov, Fundamentals of the Theory of Metals, Elsevier Science Publishers, B.V., North-Holland, (1988)

[22] J. Bardeen, L.N. Cooper and J.R. Schrieffer, Phys. Rev. **108**, 1175, (1957).

[23] Y. Yeshurun and A.P. Malozemoff, Phys. Rev. Lett. **60**, 2202, (1998).

[24] P. W. Anderson, Phys. Rev. Lett 9, 309, 1962; P.W. Anderson and Y.B. Kim Rev. Mod. Phys. **36**,39, (1964).

[25] M. P. A. Fisher Phys. Rev. Lett. **62**,1415,(1989).

[26] V.M. Vinokur, G. Blatter, M.V. Feigelman, V.B. Geshkenbein, and A.I. Larkin Physica C **185-189**, 276, (1991).

[27] P.L. Gammel, L. F. Schneemeyer, J. V. Waszczak and D.J. Bishop, Phys. Rev. Lett. **61**,1666, (1988).

[28] M.V. Feigel'man, V. M. Geshkeinbein, A.I. Larkin and V.M. Vinokur Phys.Rev.Lett. **63**, 2303, (1989).

[29] Yu. S. Karimov and A.D. Kikin Physica C **169**, 50 (1990).

[30] J. Wang, K. N. R Taylor, D. N. Matthews, H. K. Liu, G. J. Russel, and S. X. Dou, Physica C **180**, 307 (1991).

[31] L. P. Ma, H.C. Li and L. Li, Physica C **291**,143 (1997).

[32] K.A. Müller, M. Takashiga and J.G. Bednorz, Phys. Rev. Lett. **58**, 1143 (1987).

[33] Z. L. Xiao, E. Y. Andrei and M. J. Higgins Phys. Rev. Lett. 83, 1664 (1999).

[34] H. Yetis, Transport and Relaxation Measurements in Ceramic Superconductors, Ms Thesis, (2003).

[35] A. Kiliç, K. Kiliç and O. Çetin , J. Appl. Phys. **93**,1, (2003) Virtual Journal of Appl. of Supercon., Vol 4, issue 1, (2003).

[36] Y. Paltiel, E. Zeldov, Y.N. Myasoedov, H. Shtrikman, S. Bhattacharya, M.J. Higgins, Z.L. Xiao, P. L. Gammel and D.J. Bishop, Nature **403**, 398, (2000).

[37] K. Kiliç, A. Kiliç, H. Yetiş and O. Çetin, J. Appl. Phys., **95**, 1924, (2004).

[38] N. Gordeev, P. A. J. de Groot, M. Oussena, A. V. Volkozup, S. Pinfold, R. Langan, R. Gagnon, and L. Taillefer, Nature **385**, 324 (1997).

[39] S. N. Gordeev, P. A. J. de Groot, M. Oussena, R. M. Langan, A. P. Rassau, R. Gagnon, and L. Taillefer, Physica C **282-287**, 2033 (1997).

[40] G. D'Anna. P. L. Gammel, H. Safar, G. B. Alers, and D. J. Bishop, Phys. Rev. Lett. **75**, 3521 (1995).

[41] H. Fukuyama and P. L. Lee, Phys. Rev. B **17**, 535 (1978).

[42] R. M. Fleming and C. C. Grimes, Phys. Rev. Lett. **42**, 1423 (1979).

[43] J. Dumas, C. Schlenker, J. Markus, and R. Buder, Phys. Rev. Lett. **50**, 757 (1983).

[44] L. Pietronero and S. Strassler, Phys. Rev. B **28**, 5863 (1983).

[45] R. P. Hall and A. Zettl, Phys. Rev.B **30**, 2279 (1984).

[46] H. F. Hundley and A. Zettl, Phys. Rev. B **33**, 2883 (1986).

[47] R. M. Fleming and L. F. Schneemeyer, Phys. Rev. B **33**, 2930 (1986).

[48] S. N. Coppersmith and P. B. Littlewood, Phys. Rev. B **36**, 311 (1987).

[49] G. Grüner, Rev. Mod. Phys. **60**, 1129 (1988).

[50] S. N. Coppersmith, Phys. Rev. Lett. **65**, 1044 (1990).

[51] S. N. Coppersmith, Phys. Rev.B **44**, 2887 (1991).

[52] S. N. Coppersmith and A. J. Millis, Phys. Rev. B **44**, 7799 (1991).

[53] M. R. Sarkardei and R. L. Jacops, Phys. Rev. E **51**, 1929 (1995).

[54] K. L. Ringland, A. C. Finnefrock, Y. Li, J. D. Brock, S. G. Lemay, and R. E. Thorne, Phys. Rev. Lett. **82**, 1923 (1999).

[55] M. Karttunen, M. Haataja, K. R. Elder, and M. Grant, Phys. Rev. Lett **83**, 3518 (1999).

[56] W. K. Kwok , G. W. Craptree, J. A. Fendrich, and L. M. Paulius, Physica C **293**, 111 (1997).

[57] R. B. Stephens, Cryogenics, **29**, 399 (1989).

[58] H. Kliem, A. Weyers and J. Lützner, J. Appl. Phys. **63**, 1534 (1990).

[59] A. Kilic, Supercond. Sci. Technol. **8**, 497 (1995).

[60] A.-C Shi and A.J. Berlinsky, Phys. Rev. Lett. **67**,1926 (1991).

[61] C. Reichhardt, J. Groth, C. J. Olson, S. B. Field, and F. Nori, Phys. Rev. B **54**, 16108 (1996).

[62] C. J. Olson, C. Reichhardt, J. Groth, S. B. Field, and F. Nori, Physica C **290**, 89 (1997).

[63] C. J. Olson, C. Reichhardt, and F. Nori, Phys. Rev. Lett. **81**, 3757 (1998).

[64] A.Kiliç, K. Kiliç, and O Çetin, Physica C **384**, 321 (2003).

[65] S. Senoussi, J. Phys. (Paris) III, **2**, 1041 (1992).

[66] G. Blatter, M.V. Feigel'man, V.B. Geshkenbein, A.I. Larkin and V.M. Vinokur, Rev. of Mod. Phys. vol. **66**, No.4, 1125, (1994).